Landslide hazard Zonation and Slope Instability Assessment by using Optical and InSAR Remote Sensing: The case of Arbaminch-Gidole Road, Southern Ethiopia

Filagot Mengistu

A Thesis Submitted to

School of Earth Sciences

Advisor: Dr. K.V. Suryabhagavan

Presented in Partial Fulfilment of the requirements for the Degree of Masters of Science (Remote Sensing and Geoinformatics)

ADDIS ABABA UNIVERSITY

Addis Ababa, Ethiopia

May, 2018

Landslide hazard Zonation and Slope Instability Assessment by using Optical and InSAR Remote Sensing: The case of Arbaminch-Gidole Road, Southern Ethiopia

Filagot Mengistu

A Thesis Submitted to

School of Earth Sciences

Advisor: Dr. K.V. Suryabhagavan

Presented in Partial Fulfilment of the requirements for the Degree of Masters of Science (Remote Sensing and Geoinformatics)

ADDIS ABABA UNIVERSITY

Addis Ababa, Ethiopia

May, 2018

SIGNATURE PAGE

Addis Ababa University
School of Graduate Studies

This is to certify that the thesis prepared by **Filagot Mengistu**, entitled: *Landslide Hazard Zonation and Slope Instability Assessment by using Optical and InSAR Remote Sensing: the case of Arbaminch-Gidole Road, Southern Ethiopia* and submitted in partial fulfillment of the requirements for the Degree of Master of Science (Remote sensing and Geo-informatics) complies with the regulations of the University and meets the accepted standards with respect to originality and quality.

Signed by the Examining Committee:

Examiner _____ Signature _____ Date _____

Examiner _____ Signature _____ Date _____

Advisor _____ Signature _____ Date _____

Co-Advisor _____ Signature _____ Date _____

_____
Chair of School or Graduate Program Coordinator

ABSTRACT

Landslide Hazard Zonation and Slope Instability Assessment by using Optical and InSAR Remote Sensing: the case of Arbaminch-Gidole Road, Southern Ethiopia

Filagot Mengistu, Msc. Thesis

Addis Ababa University, May 2018.

In the present study landslide hazard zonation and slope instability assessment were carried out in and around Gidole Town in Southern Ethiopia. The main objective of the study was to map landslide hazard zone using Information Value Bivariat statistical model and assess the slope instability using InSAR approach. For landslide hazard zonation of the study area six causative factors namely; aspect, slope angle, elevation, slope material, Normalized Deference Vegetation Index (NDVI) and land-use and land-cover were considered. The landslide inventory mapping for the present study area was carried out through field observations and Google Earth image interpretation. Later, Information value was calculated based on the influence of causative factors on past landslide. The distribution of landslide over each causative factor maps was obtained and analyzed. Weights for the class with in these causative factor maps was obtained using information value model. Distribution of landslide in the study area was largely governed by aspect of southwest facing, slope angel of 30-45^{o}, elevation of 1815–2150m, NDVI of 0.27−0.37, slope material of colluvial deposit and land-use and land-cover of agricultural land. The landslide hazard zonation map shows that 78.38km^2 (36.3%) area fall within very low hazard (VLH) zone, 72.85km^2 (34.2%) of the area fall within low hazard (LH) zone, 12.78 km^2 (6.6%), 32.72 km^2 (15.4%) and 15.89 km^2 (7.5%) of the area falls into very high hazard (VHH), high hazard (HH) and moderate hazard (MH), respectively. Further, validation of LHZ map with past landslide inventory data shows that 92.3% of the existing landslides fall in very high hazard (VHH) and high hazard (VHH) zone. Thus, it can safely be concluded that the hazard zones delineated in the present study validates with the past landslide data and the potential zone depicted can reasonably be applied for the safe planning of the area. Further, the landslide activities in the study area were studied using Persistent Scatterer -Interferometry synthetic Aperture method. For the analysis radar image was acquired by the Sentinel Satellite for the period 2014−2018. The result of PS-InSAR processing indicates the average displacement located in the study area has gradually increasing starting from 15.3mm/yr. to -19.2 mm/yr. The result of the study area represented in terms of vertical displacement from the satellite Line of sight. Negative displacement indicates that the land surface is moving away from the satellite line of sight and the positive sign indicate the area is moving towards line of sight.

Key words: Landslide, Gidole, Landslide hazard zone, PS-InSAR, Persistent Scattered

*****

ACKNOWLEDGEMENTS

First and foremost, thanks to God the Almighty, for his blessings throughout my work to complete the research successfully.

I would like to express my sincere gratitude to my advisor Dr. K.V. Suryabhagavan, for his valuable guidance, sacrificed his time by reading and correcting my thesis and constant support throughout the whole study period.

I really want to give my thanks to my Co-advisor Dr. Tarun K. Raghuvanshi, for his guidance, encouragement, teaching me the style of scientific writing and constructive comments.

I would like to thank Addis Ababa University, Institute of Geophysics, Space Science and Astronomy (IGSSA) for providing me the opportunity to pursue MSc at AAU.

My appreciation also goes to all members of IGSSA, for their kindness, guidance, financial, logistic and equipment support during field work and creating a wonderful place for research activities. Without their passionate participation and input the research could not have been successfully conducted.

I would also like to thank School of Earth Science for their financial support for this study.

I express my thanks to Ethiopian Meteorological Agency, Ethiopian Mapping Agency, Geological Survey of Ethiopia, USGS and ESA for their providing valuable data and satellite images.

Finally, I must express my profound gratitude to my classmate's, parents and my daughter Abigya for providing me with unfailing support, understanding and continuous encouragement throughout my years of study and through the process of researching and writing this thesis. This accomplishment would not have been possible without them. Thank you.

Filagot Mengistu

*****

TABLE OF CONTENTS

LIST OF FIGURES

LIST OF TABLES

LIST OF PLATES

ABBREVIATIONS

ANN	−	Artificial Neural Network
DEM	−	Digital Elevation Model
EO	−	Earth Obseravtion
ESA	−	European Space Agency
GIS	−	Geographic Information System
GPS	−	Global Positioning System
GSE	−	Geological Survey of Ethiopia
IFG	−	Interfrogram
IGSSA	−	Institute of Geophysics Space Science and Astronomy
InSAR	−	Interferometry Synthetic Aperture Radar
IV	−	Information Value
IW	−	Interfrometiric wide-swath
LHEF	−	Landslide Hazard Evaluation Factors
LHZ	−	Landslide Hazard Zonation
LOS	−	Line Of Sight
LULC	−	Land-Use and Land- Cover
NDVI	−	Normalized Difference Vegetation Index
OLI	−	Operational Land Imagery
PS	−	Persistence Scattered
PS-InSAR	−	Persistence Scattered-Interferometry Synthetic Aperture Radar
SAR	−	Synthetic Aperture Radar
SBAS	−	Small Baseline Subset
SLC	−	Single Look Complex
SNAP	−	Sentinel Application Platform
SNNPR	−	South National And Nationalities People Region
SRTM	−	Shuttle Radar Topography Mission
SSEP	−	Slope Susceptibility Evaluation Parameter
StaMPS	−	Stanford Method of Persistent Scatterers
TOPS	−	Terrain Observation with progressive Scan
USGS	−	United States Geological Survey

CHAPTER ONE INTRODUCTION

1.1 Background

Landslides are the major mass wasting processes and landscape building factors in mountainous terrains. Community living within mountainous environment may be at risk due to landslide disaster triggered by both manmade activities, such as: mining, road cutting, and urbanization and natural causes such as: earthquake and extreme rainfall (Martha *et al.*, 2010). Landslide hazard is becoming serious environmental constraints for the developmental activities in the highlands of Ethiopia. With the current infrastructure development, urbanization, rural development, and with the present landslide management system, it is predictable that the frequency and magnitude of landslide and losses due to such hazards would continue to increase (Bekele Abebe *et al*., 2010; Kifle Woldearegay, 2013; Tilahun Hamza and Raghuvanshi, 2017).

According to Bekele Abebe *et al.* (2010), the rate of landslides has been increasing in the recent times due to rugged morphology, high relief energy and the nature of out-cropping rocks. The triggering factors are basically related with rainfall and human interventions, such as: the rapid step of developments in hilly regions, lack of proper engineering geological investigation, any construction activities: especially roads can be the cause of small or huge landslides, like in the case of the present study area, and subsequent damage to human life, general land form and properties.

Landslide hazard assessment and susceptibility maps are a basis for strategic and regional planning for landslide hazard mitigation work (Anbalagan, 1992; Raghuvanshi*et al.*, 2014). Landslide hazard maps have a greater value to development planning as they present a spatial division of the ground in to areas of different level of potential landslide hazard zones and it provides the essential framework for land use planning and development of proper engineering practices (Anbalagan, 1992; Gemechis Chemindi et al., 2017).

The availability of a new generation of high resolution optical satellite imageries such as: Worldview, SPOT-5, IKONOS, Landsat 8 OLI, Sentinel 1A and Sentinel 2A has resulted in to a paradigm shift in the use of Earth observation data for landslide studies. The number of such satellites is increasing year by year (Van Westen *et al.*, 2008) which reduces the revisit time and thus has led to their increased preference over Aerial photographs for landslide

detection using visual interpretation technique. Change detection and image fusion are example of such methods used to identify landslide automatically (Nichol and Wong, 2005).

Space-borne Interferometric Synthetic Aperture Radar (InSAR) has developed rapidly over the past 20 years and has established to be a valuable tool for topographic mapping and surface deformation measurements (Hanssen, 2001). Because of its dense spatial coverage and competitive accuracy, InSAR has now become one of the most preferred geodetic methods to study surface deformation associated with slow-moving landslides (Rott*et al.*, 1999).

1.2 Problem statement

Gidole is a well known landslide prone area in Southwestern Ethiopia, and because of this both the natural environment and built-up infrastructures are frequently exposed to sever damages. Recently in relation to the construction of the Arbaminch-Gidole road a massive landslide has occurred that has forced to abandon the project. Besides, the local communities living in the problematic areas were resettled to the neighboring villages. Thus, development of infrastructures in and across this area requires detailed assessment of the surface and subsurface conditions. So far, some geophysical and geological studies have been conducted, nevertheless, due to the ruggedness of the topography and other logistic issues, conducting investigation in this area by surface survey techniques is practically difficult. Therefore, such surveys should be supported by remote sensing techniques which may provide effective information within a short period of time and with minimum financial inputs.

Therefore, the present study has utilized an appropriate procedure and techniques to identify landslide hazard zones, besides it has also assessed the rate of deformation by using InSAR data. These methods are important to provide landslide specification information for the extraction of fast and accurate results that will help in decision making and facilitates in implementing disaster management strategies.

1.3 Objectives

1.3.1 General objective

The main objective of the present research is to identify landslide Hazard areas and to assess ground movement by using optical and radar satellite images.

1.3.2 Specific objectives1

The specific objectives of the study were:

(i) To carry out landslide Inventory from satellite images.

(ii) To determine the rate of deformation by using InSAR Time-series analysis techniques.

(iii) To produce landslide hazard zonation map.

(iv) To generate surface displacement map.

1.4 Significance of the study

The rates of ground movement and the settlement of the residential area, just downstream of the Gidole landslide are not well known. Therefore, monitoring of ground movement and settlement is essential to assess the progressive deformation of this potentially dangerous slope. This is necessary to mitigate any damage caused to the people and to the infrastructure by sudden slope failure. Therefore, present research study is particularly designed to analyze the past and current rate of slope movement due to active landslide zone by utilizing SAR data using InSAR techniques. Because of the complicated nature of the landslide phenomenon, information about the previous activity of the slope could help for better understanding in recognizing effective components that are involved in probable slope creeping. The methods applied in the present study may provide a perspective and vital information that may be utilized by the relevant authority or department to apply the approach for landslide monitoring and mitigation strategy.

1.5 Organization of the thesis

This thesis is organized in to seven chapters. The first chapter is the introduction which includes the background, the research problem, objectives and significant of the study. The second chapter covers an overview of the study area. Chapter three includes work of previous researchers about the theoretical background for the landslide, landslide hazard zonation and InSAR methods. Chapter four describes the methodology of the research work. Chapter five describes the data collection, processing and analysis of the different methods of the results. Chapter six covers the discussion of the results and the last chapter contains conclusions and recommendations made through the present study.

*****

CHAPTER TWO AN OVERVIEW OF THE STUDY AREA

2.1 Description of the study area

The study area selected for the present research falls in SNNPR Dirashe special Woreda Gidole Town, Southwestern Ethiopia, which is about 580 km far from Addis Ababa. It lies close to the western margin of the main Ethiopian Rift Valley. The study area is defined by the co-ordinates 5º 32' 30"to5º 43' 30" N latitude and 37º 17' 30" to 37º 31' 00" E Longitude, covering a total area of 213 km^2 (Fig 2.1). The elevation of the study area, in general, ranges from 1104 to 2562m. The study area forms a part in the southern Ethiopian plateau and is bounded by the Rift from the west.

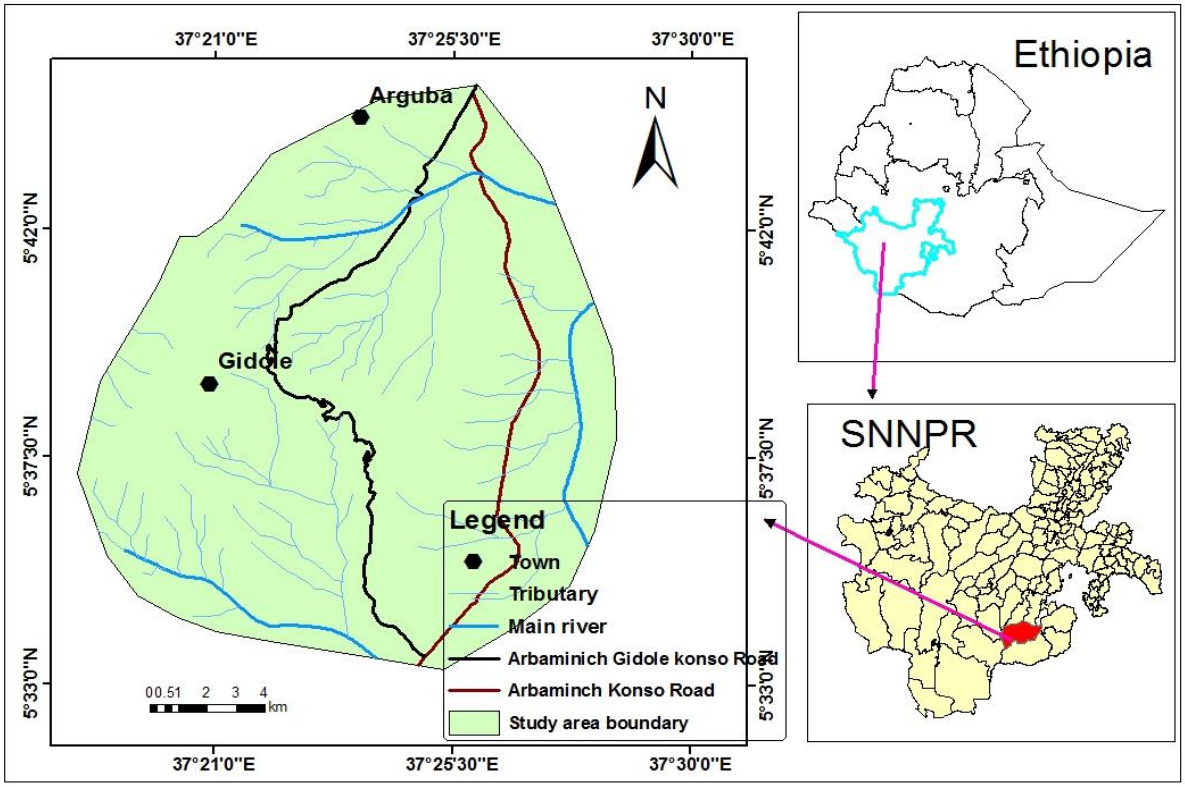

Fig.2.1 Location map of the study area

As the area is covered by both soft rocks and unconsolidated soil deposits and associated hydrogeological setup, it is prone to landslide hazards. The landslide activities mainly occurred in the area during the construction of asphalt road which is supposed to pass through the Gidole Town. As a result of this road alignment and construction old landslides in the area were reactivated and at the same time new landslides have also developed which has endangered both the road and the other infrastructure and population in the areas. The main landslide is located along the Arbaminch-Gidole-Konso road and the total length of the road

is 32.36km, it has greatly suffered by environmental problems apparently extends to relatively deep in to the surface, at least to more than 50m.

2.1.1 Climate condition

The study area is characterized by extreme variation in topography. The study area lies in the humid to semiarid areas which are classified as having average annual rainfall up to 1404.9 mm during 10 years period from 2008 up to 2017 (EMA, 2017). The highest monthly average precipitation recorded was 198.4 mm in the month of May. From March to September the area receives high rainfall whereas from October to February it receives low rainfall (Fig. 2.2.).

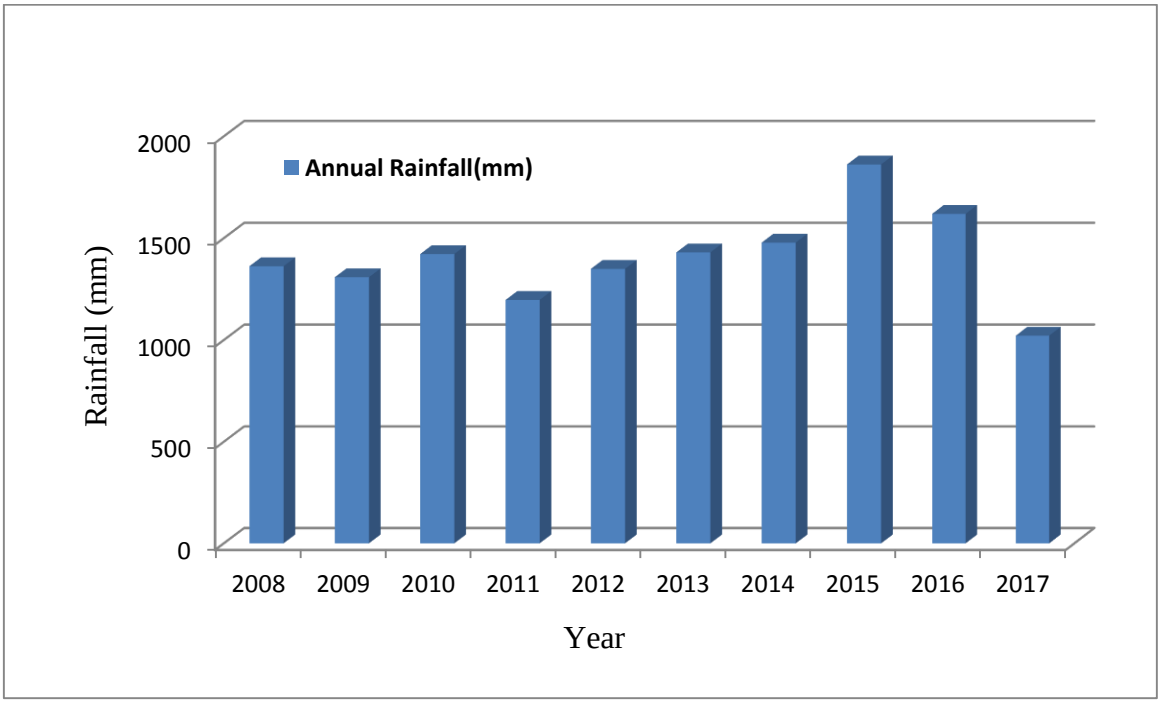

Fig. 2.2 Annual rainfall of the study area (2008−2017)

2.1.2 Population and Settlement

The Dirashe live on the mountains south of Chamo Lake in SNNPR Dirashe special Woreda. The present administrative town is Gidole. Based on data from Central Statistical Agency in 2005, Gidole has an estimated total population of 14,799. The area has many springs, but forests are becoming scarce. The town is named after the Gidole or Gardulla people, an ethnic group inhabiting southern Ethiopia known as the Dirashe. The language belongs to the lowland east Cushitic group with Konso and Oromo. Oromo and Amharic are also spoken in the administrative center. Amharic is the language of instruction. Most of the people are farmers, using hillside terraces for soil and water conservation. The Dirashe also cultivate the

lowlands to the south and east of the mountains. The main staple food is sorghum, which is stored in underground chambers for as many as ten years. Also, Teff, Maize, Barley, Oats, Ensete, beans and peas, along with vegetables and fruit (banana, lime) are grown in the area. Cattle, goats and sheep are kept for meat; beehives for honey. Donkeys are used to transport goods (https://joshuaproject.net/people_groups/11887/ET).

2.2 Geology of the study area

The geology of Gidole area is characterized by lower Precambrian, basal sandstone, basaltic volcanic and associated silicic units that have erupted in the form of sheet and central type of volcanoes along the extensional rift structures (Davidson, 1983). According to Davidson (1983), the Precambrian basement rocks are predominantly gneisses which are intruded by syn tectonic and post tectonic granitoid, gabbroic and ultramafic massifs. Metamorphic grade is mainly middle to upper amphibolitic facies, but has reached granulite facies in places and migmatized parts are also present. The Tertiary pre-rift succession underlies the northern part of the area in Nyalibong hills, Mago Mountain, Gazer and Gidole areas; in eastern part of konso highlands, Teltele and Bulal plains and in the most southern part along, the Kenya border between Fejej and Minogelti. The basalt dominates the lower part of the section, followed by thick units of salic rocks. A total thickness of the formation varies from 2000 to 3000 m from Nyalibong hills to Gidole highlands, respectively (Jiri, 1987). The Gidole area is covered with various type of lithological formation such as pyroclastic deposit, basal sandstone, basalt, colluvial deposit, metamorphic rock and alluvium sand and clay (Fig 2.3).

2.2.1 Basalt

This lithology covers a large part of the study area. It is highly fractured and slightly weathered. It is grayish and at some places this unit is intercalated with felsic rocks. The exposure on the foot of the ridge is light grey, slightly vesicular, columnar jointed and more or less horizontally layered. The basalt outcrop exposed at the junction of the existing and abandoned roads is also light grey, but highly weathered (Plate 2.1).

2.2.2 Pyroclastic flow deposit

This deposit overlay the basalt unit. It is both yellowish and grey. At other overlays it also overlay the sandstone unit. The bottom layer however is characterized by poorly sorting, poor or no bedding, discontinuous trains of large fragments and alternating coarse- to fine-grained layers (Plate 2.2).

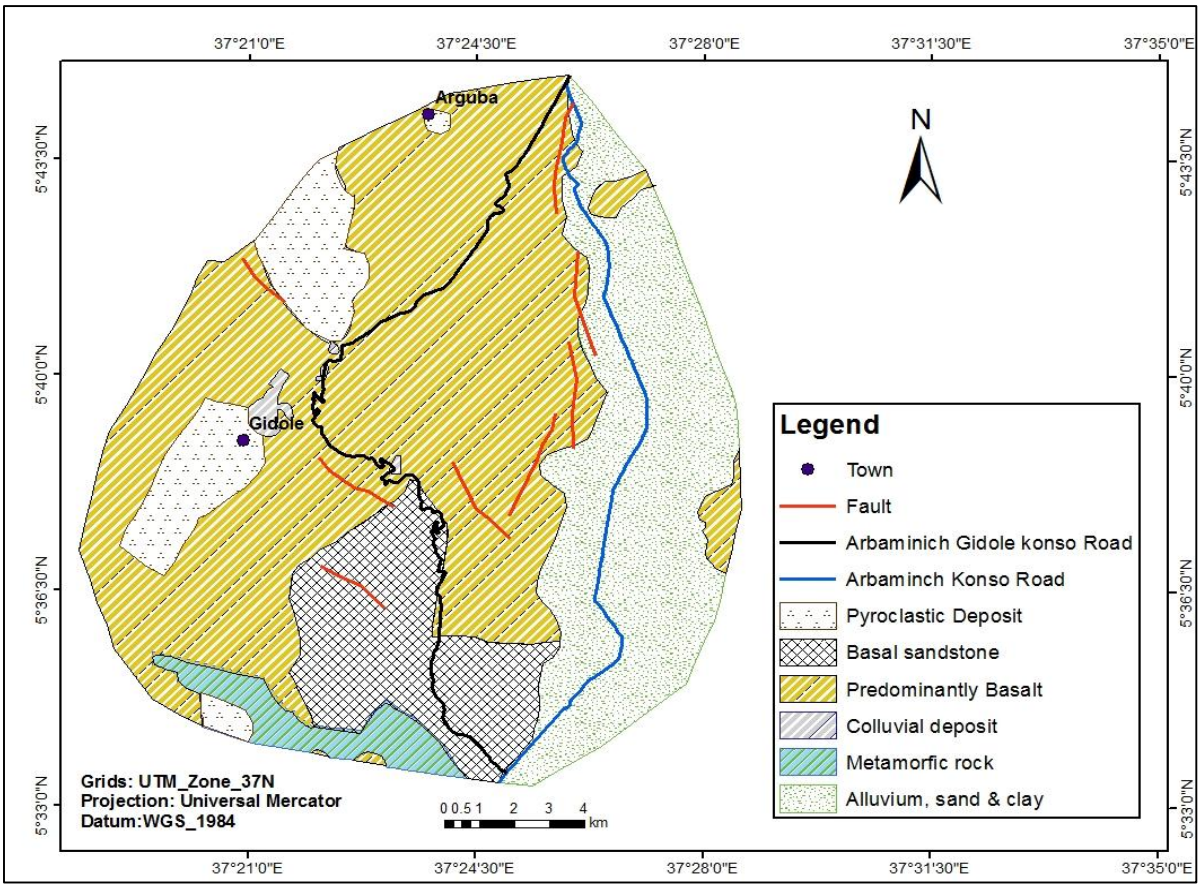

(Source: after modified from GSE, 2014)

Fig. 2.3 Geological map of the study area

Plate 2.1 Weathered basalt

Plate 2.2 Pyroclastic flow deposit

2.2.3 Colluvial deposits

Colluvial deposit founded in the study area is composed of gravel, boulder, block and some sand or soil of unsorted, un-stratified and heterogeneous mixture ranging in size from pebble to big boulders and compositionally from rhyolite to basalt transported by landslides

(Plate2.3). The colluvial deposit found underlying the basalt unit is responsible for new and the old landslides. Colluvial deposits that are formed from old landslides are distributed covering most of the slope areas starting from the top to the lower parts of the Gidole mountain. The colluvial material is characterized by scarps and ponds resulting from the sliding of colluvial material. Rivers of the area are generally filled by debris flows of new and old landslides.

2.2.3 Basal Sandstone

The lower most rock under the volcanic pile is the basal sandstone. The reddish material is the basal sand stone at the eastern tip of the abandoned road and is 3 to 4 m thick, medium to coarse grained and thickly bedded. It is reddish and texturally matured. The bottom part of the bedding is highly weathered, reddish to brown and consists of thin layers of sand and sandy silt (Plate 2.4).

Plate 2.3 Colluvial deposit

Plate 2.4 Basal sandstone

2.3 Geological structure of the study area

2.3.1 Faults and Joints

Faults in the study area are normal faults that generally strike NE−SW and NW−SE are common in the eastern part of Gidole highland (Fig 2.4). Fault map of the study area is extracted from Sentinel 1A radar image. The joints observed in the study area are columnar joints (Plate 2.5). It is highly fractured and weathered. The presence of these joints between each block and the weakening of rock mass by penetrating water can be one factor for the rock toppling in the study area.

Plate 2.5 Columnar joints

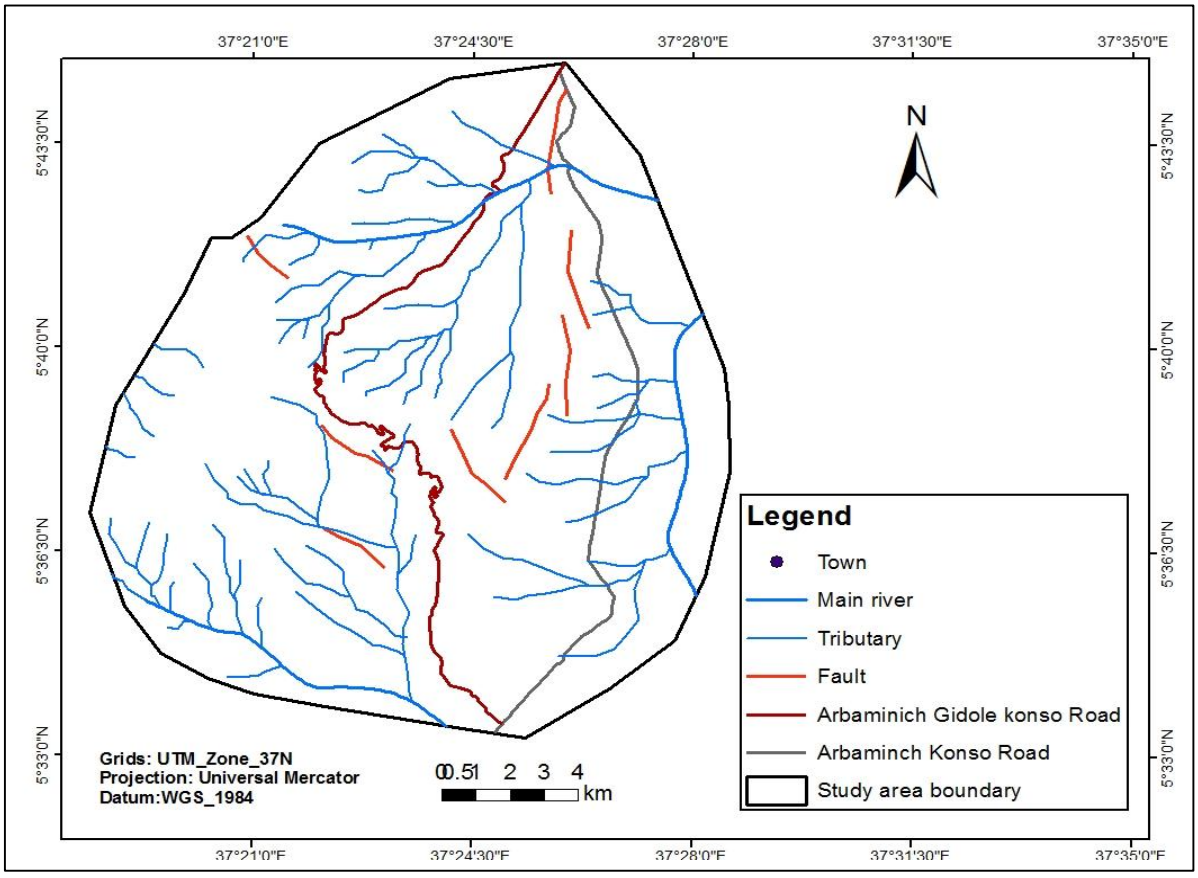

Fig. 2.4 Fault map

2.3.2 Surface crack

During field investigation different sizes of cracks have been observed at the toe of the sliding mass, agricultural lands and residential areas. The cracks have approximately 1 to 1.5m width and up to 1m depth. (Plate2.6 A and B) shows the surface cracks which affects coffee farm and agricultural land in the Village, respectively.

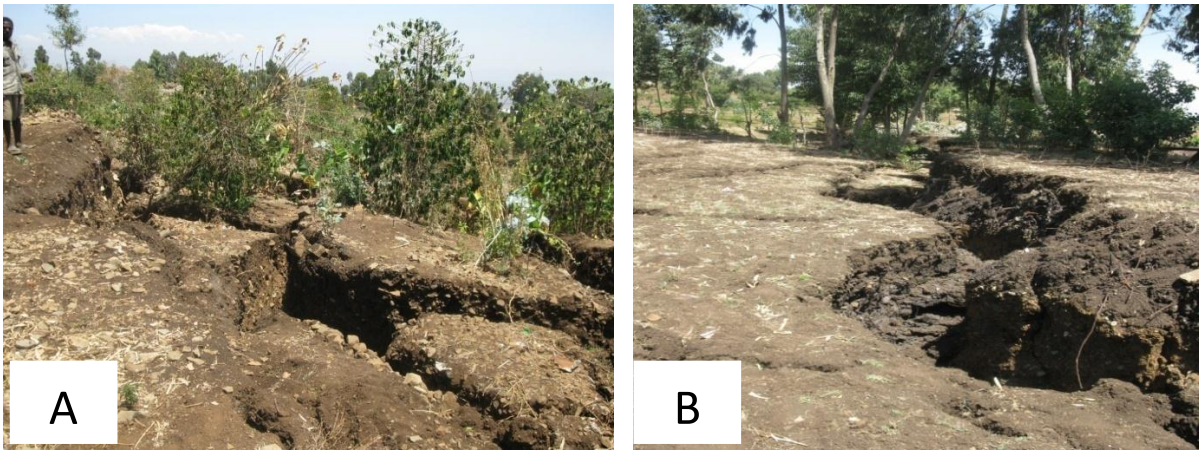

Plate 2.6 Surface cracks in the study area

2.4 Hydrogeology of the study area

During the field investigation, it was observed that many springs and ponds appeared which facilitated further landslide in the area which was formed after the landslide started along the newly constructed road (Plate2.7). The water-bearing zones in the Gidole highland and the rift escarpment are within the weathered and fractured basalt and locally in inter-bedded river gravels and unconsolidated sedimentary deposits. Therefore, groundwater migrates to the east following the faults as well as the contact zone between the weathered basalt and massive trachyte dyke (Jiri, 1987) on the western tip of the collapsed road.

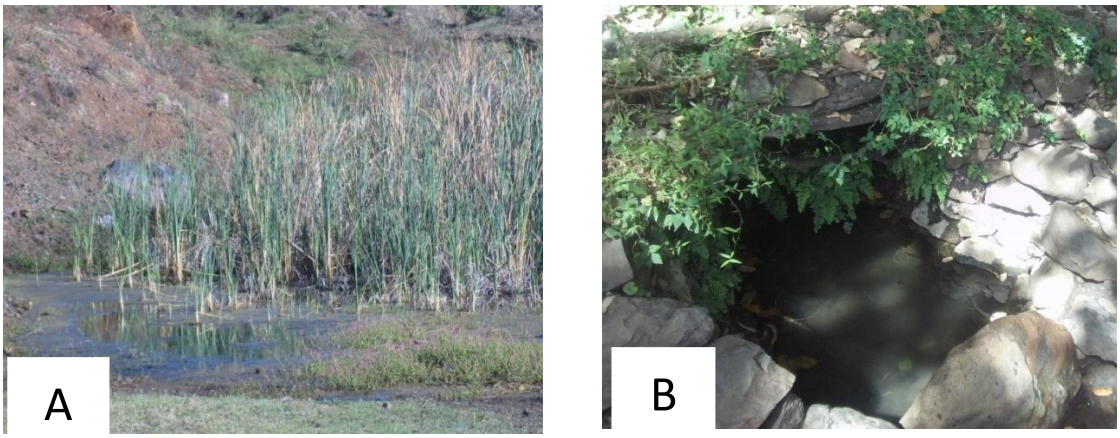

Plate 2.7 Pond appeared after the landslide occurred (A) and Spring (B)

2.5 Seismicity

As the study area is located near to the main escarpments of the rift, it is prone to different magnitude of earthquakes. As it was observed during the present study, the study area in most of the parts is covered by either colluviums or residual soil. These types of material amplify the seismic waves than the underlying bed rock.

CHAPTER THREE LITERATURE REVIEW

3.1 Landslides: An overview

Landslide, defined as the mass movement of rock, debris or earth down a slope, results in a geomorphic transformation of the Earth's surface (Cruden, 1991). Landslides are a sign of slope instability which is defined as the tendency for a slope to undergo morphologically and structurally disruptive landslide processes. It could be manifested in different and combinations of various forms, including rockfalls, rockslides, debris flow, soil slips, rock avalanches and mud-flows (Chau*et al*., 2004). Individual slope failures are generally not so huge or so costly as earthquakes, major floods, hurricanes or some other natural catastrophes. Slope failures are more widespread, and over the years they may cause more damage to properties than any other geological hazards (Varnes, 1984). The main triggering factors of landslides are rugged topography, weakness of geological structure and variation in bedrock lithology (Varnes, 1978; BekeleAbabe*et al*., 2010).The study of landslides has drawn worldwide attention mainly due to increasing awareness of the socio-economic impact of landslides, as well as the increasing pressure of urbanization on the mountain environment (Aleotti and Chowdhury, 1999).

3.2 Types of landslides

The term "landslide" describes a wide variety of processes that result in the downward and outward movement of slope-forming materials including rock, soil, artificial fill, or a combination of these thematic maps(Varnes, 1984; Highland and Bobrowsky, 2008). The materials may move by falling, toppling, sliding, spreading, or flowing. The various types of landslides can be differentiated by the kinds of material involved and the mode of movement.

3.2.1 Rock fall

Rock falls are abrupt movements of masses of large rocks or boulders whichare detached from their parent rock. They usually fall along steep slopes or cliffs. Separation occurs along discontinuities such as fractures, joints, and bedding planes and movement occurs by free-fall, bouncing, and rolling (Fig 3.1). Falls are usually influenced by gravity, mechanical weathering, and the presence of interstitial water. It is common in steep slopes, or vertical slopes also in coastal area, along rocky bank of river and streams, road cuts, and jointed, fractured and weathered bedrock (Wachal and Haduk, 2000).

3.2.2 Topple

Topple failure encompasses the forward spinning and movement of huge masses of rock, debris and earth from a slope (Varnes, 1984). This type of slope failure takes place around an axis near or at the bottom of the block of rock (Fig 3.2). It is usually caused by cracks or fracture in the bedrocks. The rate of movement ranges from extremely slow to extremely rapid and it can be destructive especially when failure is sudden(Highland and Bobrowsky, 2008).

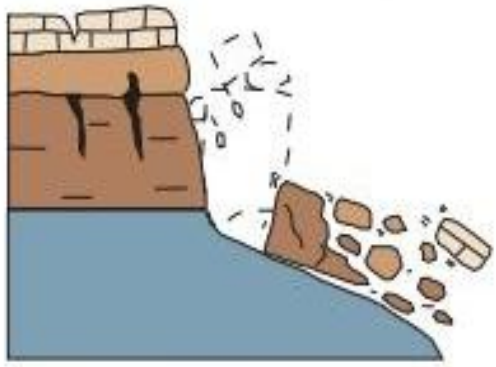

(Source: Highland and Bobrowsky, 2008)

Fig. 3.1 Rock fall **Fig. 3.2Topple**

3.2.3 Flow

Flows come in many types, such as debris flow, debris avalanche, mudflow, creep and Earth flow. Debris flow involves the rapid downhill movement of loose earth material usually with water (Fig. 3.3(B)). Debris Avalanche is similar to debris flow but has a more rapid flow (Fig 3.3(A)). In an Earth flow, the earth material is finer and is washed away leaving a depression bowl at the head (Fig 3.3 (C)). Mudslides are made up of fine silt, sand and clay material saturated with water and flowing very rapidly. Creeps are slower in nature and can be evident when electric poles and roads bend slightly (Fig 3.3 (D)). They are commonly caused by intense surface water flow, due to heavy precipitation or rapid snowmelt, which erodes and mobilizes loose soil or rock on steep slopes. They can move objects as large as houses in their downslope flow or can fill structures with a rapid accumulation of sediment and organic matter (Highland and Bobrowsky, 2008).

3.2.4 Slide

This is a kind of mass movement whereby the sliding material breakaways from underlying stable material. Slides may be translational or rotational. In a translational slide the landslide

mass moves along a roughly planar surface with little rotational or backward tilting (Fig 3.4 (A)). In a rotational slide, a slide in which the surface of rupture is curved concavely upward and the slide movement is roughly rotational about an axis that is parallel to the ground surface and transverse across the slide (Varnes, 1978)(Fig 2.4 (B)).They are common in loose unconsolidated soils and their rate of movement ranges from extremely slow to moderately fast and it can be damage structures but not life if the movement is slow (Highland and Bobrowsky, 2008).

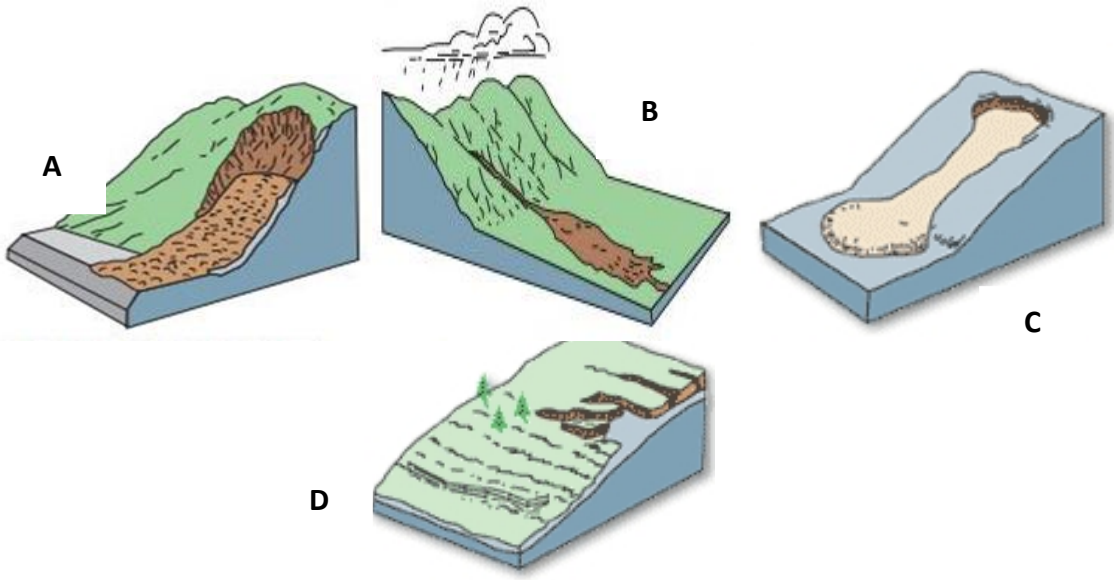

(Source: Highland and Bobrowsky, 2008)

Fig. 3.3 Debris Avalanche (A), Debris flow(B), Earth flow(C) and Creep (D)

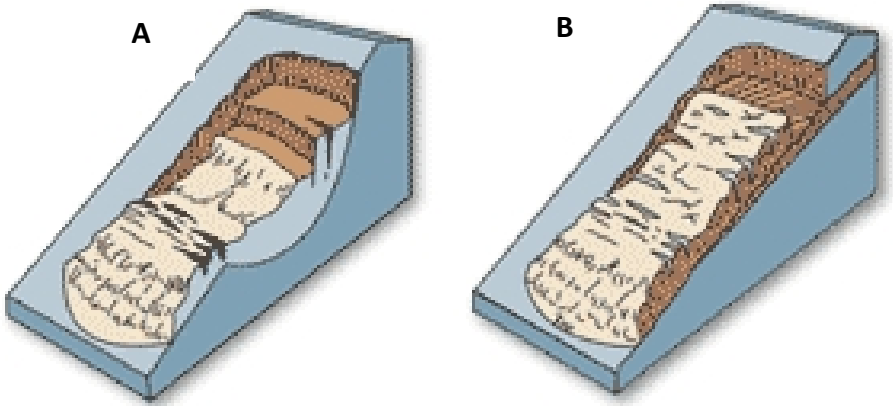

(Source: Highland and Bobrowsky, 2008)

Fig. 3.4Rotational slide (A), Transitional slide(B)

3.2.5 Lateral Spread

Lateral spreads are distinctive because they usually occur on very gentle slopes or flat terrain. The dominant mode of movement is lateral extension accompanied by shear or tensile fractures (Fig 3.5). The failure is caused by liquefaction, the process whereby saturated, loose, cohesion less sediments (usually sands and silts) are transformed from a solid into a liquefied state. Failure is usually triggered by rapid ground motion, such as that of experienced during an earthquake, but can also be artificially induced. When coherent material, either bedrock or soil, rests on materials that liquefy, the upper units may undergo fracturing, extension and then subside, translate, rotate, disintegrate, or liquefy and flow off. Lateral spreading in fine-grained materials on shallow slopes is usually progressive.Lateral spreads typically damage pipelines, utilities, bridges, and other structures having shallow foundations (Highland and Bobrowsky, 2008).

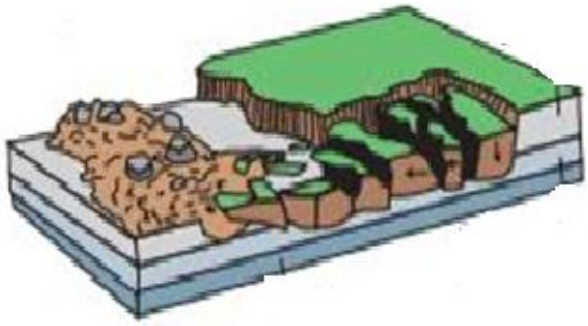

(Source: Highland and Bobrowsky, 2008)

Fig. 3.5 Lateral Spread

3.3 Landslide Inventory

Landslide hazard and risk management begins with comprehensive landslide Inventory, which serves as a basis to understand their spatial and temporal occurrences (Guzzetti*et al.*, 2000; Brardinoni*et al.*, 2003). Inventory of landslides includes recognition and classification of landslide based on type of material and type of movement (Varnes,1978). Earth observation data are increasingly used for landslide mapping, with automatic methods being preferable over manual approach for obtaining quicker result over large area (Barlow*et al.*, 2006; Borghui*set al.*, 2007).

3.4 Landslide hazard zonation approaches

Landslide hazard zonation is an important step in landslide investigation, landslide risk management and catastrophic loss reduction and assists in the development of guidelines for

sustainable land use planning. Landslide hazard zonation is used to identify potential landslide hazard areas or other mass movements, establish a relationship between landslide and triggering factors, ranking according to the degrees of actual or potential landslide susceptibility, and to predict the landslide hazard in the future. (TenalemAyenew and Barbieri, 2005; TilahunHamza and Raghuvanshi, 2017).

Over last three decades LHZ has been carried out in different parts of the world. Several approaches have been developed for LHZ such as inventory-based mapping, heuristic approach, probabilistic assessment, deterministic approach, statistical analysis and multi criteria decision making approach (Raghuvanshi*et al*., 2014; GemechisChimindi*et al*., 2017; TilahunHamza and Raghuvanshi, 2017).

3.4.1 Inventory based mapping approach

Inventory based mapping is one of the simplest qualitative approaches of LHZ mapping. In this analysis, landslide inventory maps are produced which portray spatial and temporal patterns of landslide distribution, type of movement, rate of movement, type of displaced material (earth, debris or rock) etc. Landslide data are obtained through field survey mapping, historical records, satellite images and aerial photo interpretation. Landslide inventory map also shows a slope failure by a single event or they may show cumulative effects of many events (Cruden, 1991; Guzzetti*et al*., 2005; Raghuvanshi*et al*., 2014).Further, application of such expert evaluation techniques are more practical, simple in application and provide much more realistic field data well supported by experience of an expert in relatively less time (Raghuvanshi*et al*., 2014).

3.4.2 Statistical approach

In the last few years the approach towards LHZ has been changed from heuristic (knowledge based) approach to data driven approach (statistical approach) to minimize subjectivity in weightage assignment procedure and produce more objective and reproducible results (Kanungo*et al*., 2009). Methods based on statistical analysis of geo-environmental factors related to landslide occurrence are preferred. The statistical methods for LHZ can be grouped into two *viz*. bi-variate statistical analysis and multi-variate statistical analysis. The statistical methods are used to evaluate spatial landslide instability based on relationship between the landslide activities and their causative factors (Carrara*et al*., 1992; TilahunHamza and Raghuvanshi, 2017).

3.4.2.1 Bi-variate statistical approach

The bi-variate statistical approach for landslide hazard zonation compares each factor map (slope, geology, LULC, aspect and elevation) to the existing landslide distribution (Kanungo*et al*., 2009).

Weights to the landslide causative factors are assigned based on landslide density. Frequency analysis approach, Information Value Model (IVM), weights of evidence model, weighted overlay model etc. are important bi-variate statistical methods used in Landslide Hazard Zone (LHZ) mapping.

3.4.2.2 Multi-variate statistical approach

Multi-variatetechniques for landslide hazard zonation correlate all the factors among themselves and factors with the landslide occurrence simultaneously (Bonham-Carter, 1994;Kanungo*et al*., 2009).

These methods calculate percentage of landslide area for each pixel and landslide absence - presence data layer is produced followed by the application of multivariate statistical method for reclassification of hazard for the given area. Logistic regression model, discriminate analysis, multiple regression models, conditional analysis, Artificial Neural Networks (ANN) are commonly used methods for LHZ mapping (Brenning, 2005; Kanungo*et al*., 2009; Varmuza and Filzomoser, 2009).

3.4.3 Deterministic Approach

Deterministic approach provides landslide hazard in absolute values in the form of safety factors, or the probability (Raghuvanshi*et al*., 2015; 2014;Fall *et al*., 2006;Barredo*et al*., 2000). The deterministic analyses are quantitative and are applied to small to medium size areas at large to medium scale mapping. They also require a large amount of detailed input data and they may lead to oversimplification if such data are only partially available (Barredo*et al*., 2000; Van Westen*et al*., 2006; Raghuvanshi*et al*., 2014).

The major disadvantages of these methodsinclude the high degree of uncertainty of the input data, the high degree of parameterization required for sensitivity analysis, and the unsuitability for complex landslides, especially the landslides with complex hydrological systems.The approach can only be successful when the failure and trigger mechanisms of different landslide types are correctly identified and modeled (Wadge, 1988; Terlien, 1996).

3.5 Interferometric Synthetic Aperture Radar for deformation monitoring

3.5.1 Synthetic Aperture Radar Interferometry: Basics

Synthetic Aperture Radar (SAR) is a coherent active microwave remote sensing system which permits to reconstruct complex high resolution image of the illuminated scene. A SAR sensor, usually mounted aboard aircrafts and/or satellites, operates in a side-looking configuration and permits to measure, with high accuracy, the distance between the system moving platform and the scene surface. The received backscattered radar signal (echo) accounts for the physical characteristics of the imaged scene as well as the acquisition geometry and, after a proper processing step, it allows reconstructing high spatial resolution ground images, independently from the sensor altitude (Cumming and Wong,2005).

As an active system, the SAR provides its own illumination and is not dependent on light from the sun, thus permitting continuous day/night operation. Furthermore, neither clouds, fog nor precipitation have a significant effect on microwaves, thus allowing all-weather imaging. As a consequence of its flexibility, SAR technology mostly improved during the last years and several SAR related techniques have been developed in scientific and commercial scenarios (Berardino*et al*, 2002).

One of the major applications of the SAR technology is represented by the SAR Interferometry (InSAR) technique which exploits the phase difference, often referred to as Interferogram, between two complex-valued SAR images relevant to an investigated area acquired from slightly different orbit positions and at different times in order to retrieve geophysical parameters such as scene topography or ground deformation(Goldstein and Zebker, 1989). In particular, conventional mono-static InSAR configurations involve the use of two antennas observing the investigated scene at the same time and from different positions, spaced in the across-track direction (across-track interferometry), at different times and from the same position (along-track interferometry), at different times and from different orbital positions (repeat-pass across-track interferometry) (Moccia and Rufino, 2001; Suchandt*et al.*, 2010).

The two SAR images are generally acquired from slightly different imaging geometries. The second SLC must be precisely co-registered and resampled to the geometry of the first Single Look Complex (SLC) (Zebker and Goldstein, 1986; Sansosti*et al.*, 2006). The interferometric phase is then computed by multiplying the first SLC with the complex conjugate of the co-

registered second SLC. The resulting complex valued image is called an interferogram (IFG). Ignoring any time delays in the imaging hardware, the estimated interferometric phase can be directly related to the difference in path length to a target from the imaging platform in the line of sight (LOS) direction(Zebker and Goldstein, 1986).

Differential satellite InSAR is an invaluable tool for land displacement monitoring, particularly for the slow and very slow landslides (Hung*et al.*, 2001). Recently, the potential of a differential synthetic aperture radar approach has been investigated to study landslides by numerous research groups (Berardino*et al.*, 2003; Hilley*et al.*, 2004; Strozzi*et al.*, 2005; Colesanti and Wasowski, 2006;Rott and Nagler, 2006).

The interferometric phase measurements, however, are affected by various decorrelation phenomena (Zebker and Villasenor, 1992). The main limiting factors are atmospheric artifacts that can introduce a bias in the phase measurement (Zebker*et al.*, 1997), and temporal decorrelation that makes InSAR phase measurements unreliable over vegetated regions due to the change in relative position of the scatterers in a resolution element (Zebker and Villasenor,1992).

3.5.2 Synthetic Aperture Radar Geometry

Synthetic aperture radar is an extension of classical radar techniques developed in the first half of the 20th century. Pulse compression techniques and the synthetic aperture concept enable spatial resolutions on the order of meters with relatively small physical antennas. Space borne SAR instruments were initially used for the investigation of planetary surfaces with the first Earth orbiting SAR instrument not launched until 1978, aboard the NASA SEASAT satellite.

The principle of using space borne SARs as interferometers dates to early 1970s (Richman, 1971; Zisk, 1972) and the first terrestrial InSAR applications were in the late 1980's (Zebker and Goldstein, 1986; Goldstein and Zebker, 1987). However, it was the launch of the ESA satellite ERS-1 in 1991, leading to a large amount of SAR data suitable for InSAR becoming available that made InSAR widely applicable. SAR systems operate with a side-looking geometry and illuminate the Earth with aseries of microwave pulses. As the spacecraft moves, the illuminated footprint sweeps out a swath in the direction of movement. Interspersed with pulse transmission, the SAR detects echoes of previous pulses, scattered from the Earth(Bamler and Hartl, 1998).

Airborne and space borne SAR systems typically have a fixed side-looking antenna that illuminates a strip or swath parallel to the sensor's ground track with a series of monochromatic microwave pulses (Fig. 3.6). The platform's flight direction is called the azimuth direction and the direction of the main lobe of the transmitting antenna is called the range direction. The antenna, when inactive between transmissions of pulses, is designed to receive the scattered echoes from the illuminated surface of earlier transmitted pulses. From antenna theory, the area illuminated on the ground is inversely proportional to the physical shape and dimensions of the antenna (Skolnik, 2001).

The raw data collected by the SAR is then focused to form an image. This is achieved in the direction perpendicular to the flight direction (range) through knowledge of the time delay, and in the flight direction (azimuth) through combination of echoes from multiple locations to synthesize a large antenna aperture. In range direction, bandwidth is provided by the nature of the pulse, whereas in azimuth direction, bandwidth is provided by the variation in frequency due to the Doppler effect associated with the movement of the sensor relative to the Earth. There are various algorithms and implementations to carry out image processing, a review of which is provided by (Bamler and Hartl, 1998).

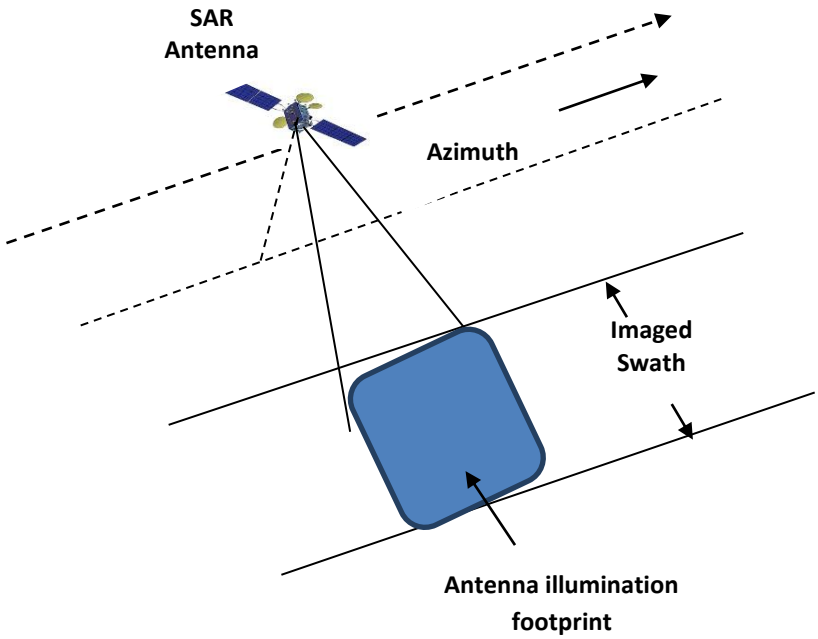

Fig. 3.6SAR Image Geometry

3.6 Previous studies on landslide in Ethiopia

Several studies have been conducted by using different approaches to assess the causes and factors that cause landslide in different parts of the country. Some of landslide studies in Ethiopia carried out by different approaches are;GemichisChimidi*et al*., 2017; TilahunHamza and Raghuvanshi 2017; BirhanuErmias*et al*., 2017; Raghuvanshi*et al*., 2015; Raghuvanshi*et al*., 2014; ShiferawAyele*et al*., 2014; KifleWoldearegay, 2013; TenalemAyenew and Barbieri, 2004; LulsegedAyalew and Yamagishi, 2004; LulsegedAyalew, 1999etc. The significant studies arepresented in the following paragraphs.

GemichisChimidi*et al*. (2017)conducted a study to carry out landslide evaluation and zonation in and around Gimbi town in western Ethiopia. This study was conducted following GIS-based statistical method. Statistical correlations between each of the causative factors and the past landslideswere established inGIS environment to rate the relative contribution of individual factor classes. The results showed that 12.2% of the study area falls in very high hazard, 30.7% in high hazard, 24.3% in moderate hazard, 23.3% in low hazard, and the remaining 9.5% in no hazard zones. Also, TilahunHamza and Raghuvanshi (2017) carried out the research to develop the landslide hazard map of the area around Jeldu district, central Ethiopia using GIS based statistical and probability approach. Raghuvanshi*et al.,* (2015) conduct the research in Meta Robi district, Oromiya Ethiopia by using grid overlay and GIS modeling approaches to prepare landslide hazard zonation map. The research showed that GIS modeling produced better landslide hazard zonation map. Also, grid overlay method is more tedious and time consuming approach.TsionAragaw (2017) conducted the research by using an integrated expert evaluation and statistical approach for landslide hazard zonation in Alemketema- Fetera route corridor, central Ethiopia. The research indicated that, in terms of area coverage 85% area is covered by high hazard in original SSEP landslide hazard zonation map where as in landslide hazard zonation may by integrated approach high hazard covers 72% of the area. In terms of total high hazard both methods provided almost similar results; original SSEP LHZ map 85% and integrated approach 82%.

According to FikireGirma*et al.,* (2015), they conducted the research on landslide hazard zonation in Ada Berga district, central Ethiopia by using GIS based statistical approach. The study used the causative factors to prepare landslide hazard zone map are curvature, slope, lithology, aspect, elevation, soil deposit, land use/land cover and ground water.Further,HenokWoldegiorgis*et al.,* (2014) made landslide hazard zonation mapping in

southern part of Abay Gorge using a landslide hazard evaluation factors (LHEF) to characterize the landslide potential zone in the area.Also,ShiferawAyele*et al.*, (2014) carried out the research to delineate landslide hazard Zone by using remote sensing and GIS approach in Abay Gorge (Gohatsion-Dejen), central Ethiopia. The study hasconsidered geology, ground water condition, drainage, slope, structure, aspect and land use/land cover as causative factors. The outcome of the research indicates that 67% landslide lie within the high hazard zone.

ZerihunDawit (2016) made the study on landslide hazard evaluation and zonation in the area KindoDidayeworeda, south west Ethiopia. In this study landslide hazard zonation of the study area was carried out by using two methods namely: Integrated slope stability susceptibility evaluation parameter and a rater based information value model approach. The findings shows that the deformation, cultivation and modifying the slopes by manmade activities in addition with high rainfall and groundwater are most influential causative parameter for the occurrence of landslide in the study area.

*****

CHAPTER FOUR METHODOLOGY

4.1 General

Several approaches have been developed for LHZ such as inventory-based mapping, heuristic approach, probabilistic assessment, deterministic approach, statistical analysis and multi criteria decision making approach (Gemechis Chimindi *et al*., 2017; Tilahun Hamza and Raghuvanshi, 2017; Raghuvanshi *et al*., 2014; Cruden, 1991; Guzzetti *et al*., 2005).

4.2 Methodology adopted for landslide Hazard Zonation

4.2.1 Information value model

Information Value (IV) model is a bivariate statistical analysis method that was developed from information theory. In this model, information values of predisposing factors are used to characterize the possibility of landslide occurrence. The information values are determined for each subclass of landslide related parameter on the basis of presence of landslide in the given mapping unit. The triggering factor maps were combined with landslide map in order to get weight of each class.

The Model has the advantage of assessing landslide susceptibility in an objective way. The method allows for the quantified prediction of susceptibility by means of a score, even on terrain units not yet affected by landslide occurrence. Each instability factor is crossed with the landslide distribution, and weighting values based on landslide densities are calculated for each parameter class, as it happens with all bivariate statistical methods. Negative values of IV mean that the presence of the variable is not relevant in landslide development. Positive values of IV indicate a relevant relationship between the presence of the variable and landslide distribution (Yin and Yan, 1988):

According to Yin and Yan (1988) weight mathematically obtained by:

$$\text{Conditional probability}=\frac{\text{Number of landslide pixels with in factor class}}{\text{Number of factor class pixels}} \quad (4.1)$$

$$\text{Prior probability}=\frac{\text{Sum of landslide pixels of the whole study area}}{\text{Sum of pixels of the whole study area}} \quad (4.2)$$

$$\text{Weight of factor class}=\frac{\text{Conditional priority}}{\text{Prior probability}} \quad (4.3)$$

$$\text{Information value} = \log(\text{Weight of factor class}) \quad (4.4)$$

Information values are assigned to each factor class to obtain weighted factor maps. These factor maps are then summed up using the raster calculator to obtain a landslide susceptibility index value for each pixel (Eq. 4.5):

$$LSI = IV_{\text{Slope Angle}} + IV_{\text{Elevation}} + IV_{\text{Aspect}} + IV_{\text{Slope Material}} + IV_{\text{NDVI}} + IV_{LULC} \quad (4.5)$$

Finally, the landslide hazard zonation map was classified into five ranked classes very low, low, moderate, high and very high hazard zone.

4.3 Methodology adopted for Slope Instability Assessment

4.3.1 InSAR time series analysis

Advanced InSAR methods such as Persistent Scattered (PS) (Greif and Vlcko, 2012) and Small Baseline Subset (SBAS) (Lanari *et al.*, 2007) which can overcome objects arising from atmospheric noise and temporal and spatial baseline decorrelation, enable us to benefit from displacement time-series analysis using a stack of SAR data. Both techniques work better in urban areas because of the high density of man-made objects, which increase the probability of discovery coherent pixels in a stack of SAR data over time. Because of the non-urban nature of the landslide area in Gidole, it is covered moderately with forest and other permanent vegetation, PS technique was used for surface displacement time-series analysis.

Long term deformation monitoring works with a special form of InSAR that is known as Persistent Scatterer Interferometry Synthetic Aperture Radar (PS-InSAR). PS-InSAR finds objects in the area of the image that produces a constant and characteristic radar reflection over time in a stack of many radar images. The PS-InSAR method was initially developed by Ferretti et al. (2000) used to estimating the time series displacement of each detected PS pixels. The StaMPS Method, developed by Hooper et al. (2007) came as an improvement the capable of finding PS pixels in urban as well as non-urban areas and also less number of interfrograms is sufficient to map the surface displacement. PS-InSAR is a multi-temporal differential InSAR technique, which analyzes long temporal stack of satellite SAR Data and provides mean velocity and time series of ground deformation on dense grids of point-wise targets, the so called Persistent Scatterers (Ferretti *et al.*, 2001). PS-InSAR work by identifying image pixels in a stack of interfrograms generated with the same master that persistently backscatter the radar signal over long time interval. The detail schematic flow chart of the methodology followed in the present study shown in (Fig 4.1).

4.4 Pre-field Investigation

During pre-field investigation secondary data and required materials were gathered from different organization. Rainfall, field equipment includes GPS, geological map was taken from Ethiopian metrological agency, Addis Ababa University, IGSSA and Geological Survey of Ethiopian, respectively. The pre-field study involved the preparation of various types of maps, such as slope angle, aspect, slope material, elevation, land-use and land-cover, NDVI and geology maps. The already available geological map and satellite imageries were studied to understand the geological setting of the areas.

4.5 During Field Investigation

During the field study, observations and measurements were made and relevant data was collected. These include data of slope material, LULC, geological structure, landslide inventory data and existing and potential landslide areas were identified. The detailed lithological and structural maps were prepared. Finally, other maps prepared during pre-field study were verified in the field and modified wherever necessary.

4.6 Post-Field Investigation

During post field investigation stage, the following activities were performed

- The thematic map of the triggering factors map and the landslide inventory map were prepared and verified.
- The thematic map of the triggering factors map and the landslide inventory map were transferred to raster to get pixel values in ArcGIS.
- Analysis of the triggering factors map and landslide inventory map was made to get the relationship between the factor classes and landslide in the study area using Information value model.
- The statistical information value maps of the triggering factors were prepared and summed to get LHZ map of the study area.
- LHZ map was verified using Landslide inventory data
- Sentinel 1A SLC radar image were processed to generate interferograms using SNAP software.

- Based on StaMPS PS-InSAR approach the most stable pixels were selected for PS processing using amplitude dispersion threshold value.
- Line of sight displacement map of the study area was prepared.
- Line of sight displacement time series map of the study area was prepared.

4.7 Software

The software that were used for the present research are ERDAS Imagine 2015, IMPACT Tools, eCognition Developer 9.1, ArcGIS 10.3.1, ESA SNAP Desktop 5.0, StaMPS v3.3b1, Snaphu-v1.4.2 and MATLAB R2017a

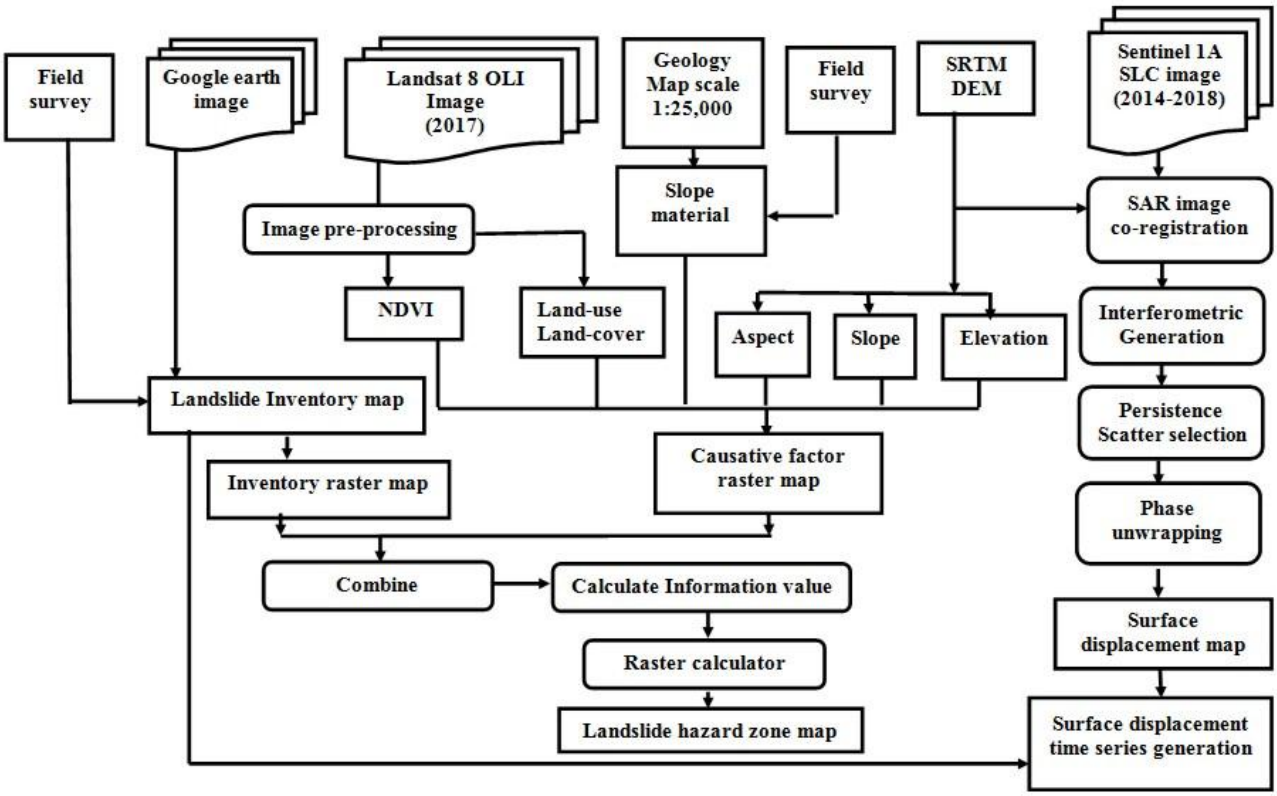

Fig. 4.1 Flow diagram showing general methodology used in the present

*****

CHAPTER FIVE DATA COLLECTION, PROCESSING ANDANALYSIS

5.1 Landslide inventory

For landslides zonation, the past and the present are the keys to the future. The principle implies that future landslide will be more likely occur under the conditions which led to past and present instability (Gemichis Chimindi *et al*., 2017; Tilahun Hamza and Raghuvanshi, 2017; Raghuvanshi *et al*., 2015; Varnes, 1984). Hence the understanding of the past landslide is essential in the assessment of landslide hazards. Landslide inventory map of the study area was prepared from the field observations (Plate 5.1) and the Google earth satellite image interpretation. In total 39 landslides of different types were recorded. These landslides occurred from 2010 to 2017 and were later used as the dataset for information value model.

5.2 Landslide hazard zonation

5.2.1 Triggering factors

The environmental factors are a collection of data that are expected to have an effect on the occurrence of landslide, and can be utilized as causal factors in the prediction of future landslides (Raghuvanshi *et al*., 2014; Van Westen*et al*., 2008; Anbalagan, 1992). The thematic maps of triggering factors including slope angle, slope material, aspect, elevation, LULC and NDVI were prepared from the SRTM DEM at 30m resolution and other vector data were prepared in Arc GIS. Slope material layer of the study area was extracted from the geological map of Ethiopia with the scale of 1:25,000 and through the field observations made during the present study. Later, all vector maps were transformed into raster data for further analysis. Details of various triggering factors layers and the data source that was used to prepare these triggering factor maps are presented in (Table 5.1).

Table 5.1 Detail of triggering layer and source

Triggering factors	Data	Data type	Data source
Landslide inventory	Google Earth image and Field observation	Polygon	Google Earth and Field observation
Elevation	SRTM DEM	30 m grid	USGS
Slope angle	SRTM DEM	30 m grid	USGS
Aspect	SRTM DEM	30 m grid	USGS
NDVI and LULC	Landsat 8 OLI 2017 Image	30 m grid	USGS
Slope material	Geology map 1:25,000	Polygon	Geological survey of Ethiopia

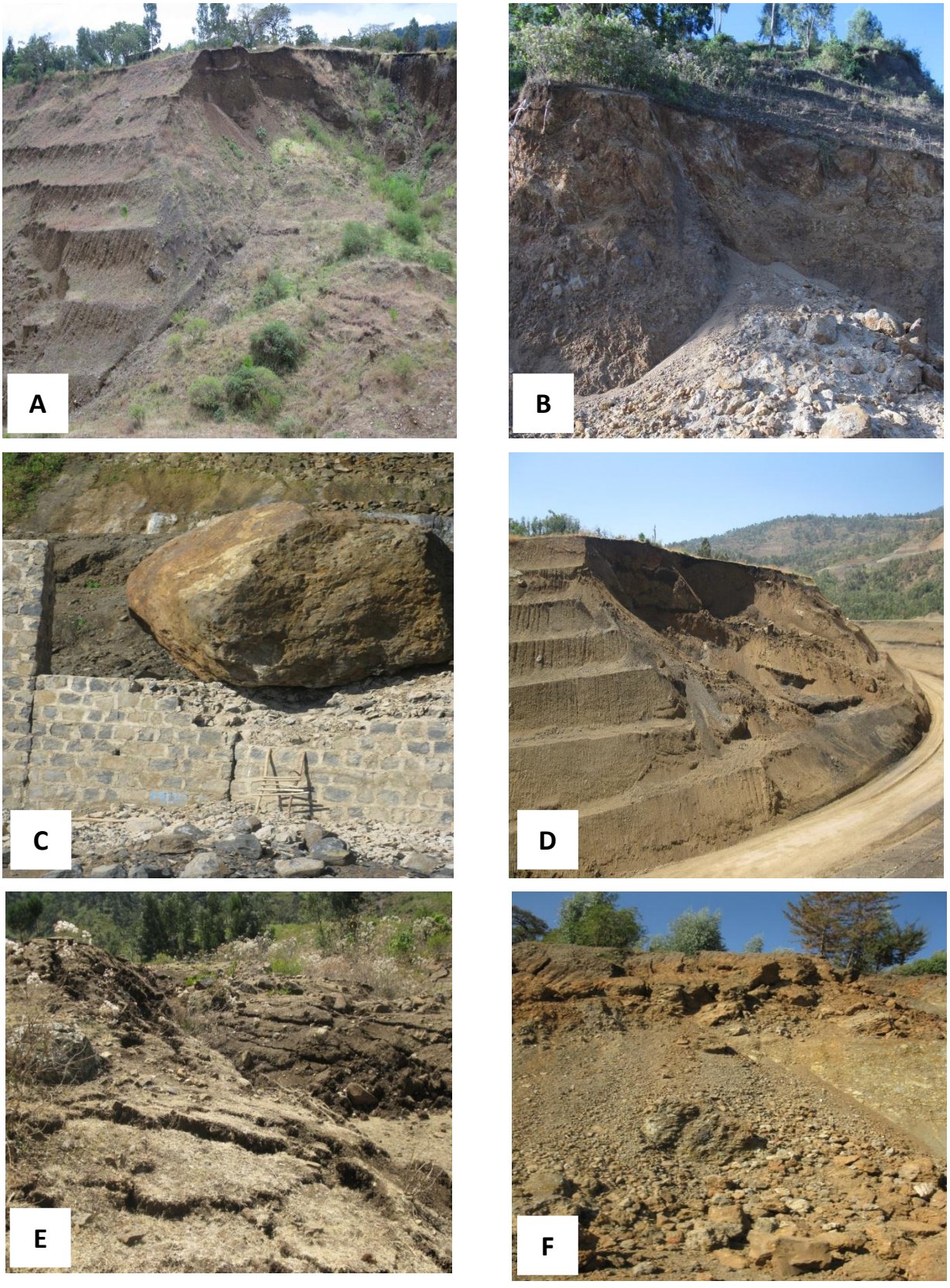

A - Rotational slide in WolayiteKebele;
B- Debris slide in the study area;
C- Rock fall damage the retaining wall;
D - Steep slope cut during road construction;
E - Earth flow damage the agriculture land
F - Debris slide in the study area

Plate 5.1 Landslides in the study area

5.2.1.1 Elevation

Elevation is a significant landslide conditioning factor because it is controlled by several geological and geomorphological processes (Ayalew*et al.*, 2005). The elevation is considered to be an important triggering factor which may possibly affect the slope material by weathering process (Raghuvanshi *et al*., 2015; Ahmed, 2009). Elevation layer was obtained from the SRTM DEM in a resolution of 30 m. As shown in Fig 5.1, the elevation of the study area ranges from 1104 to 2562m above msl.

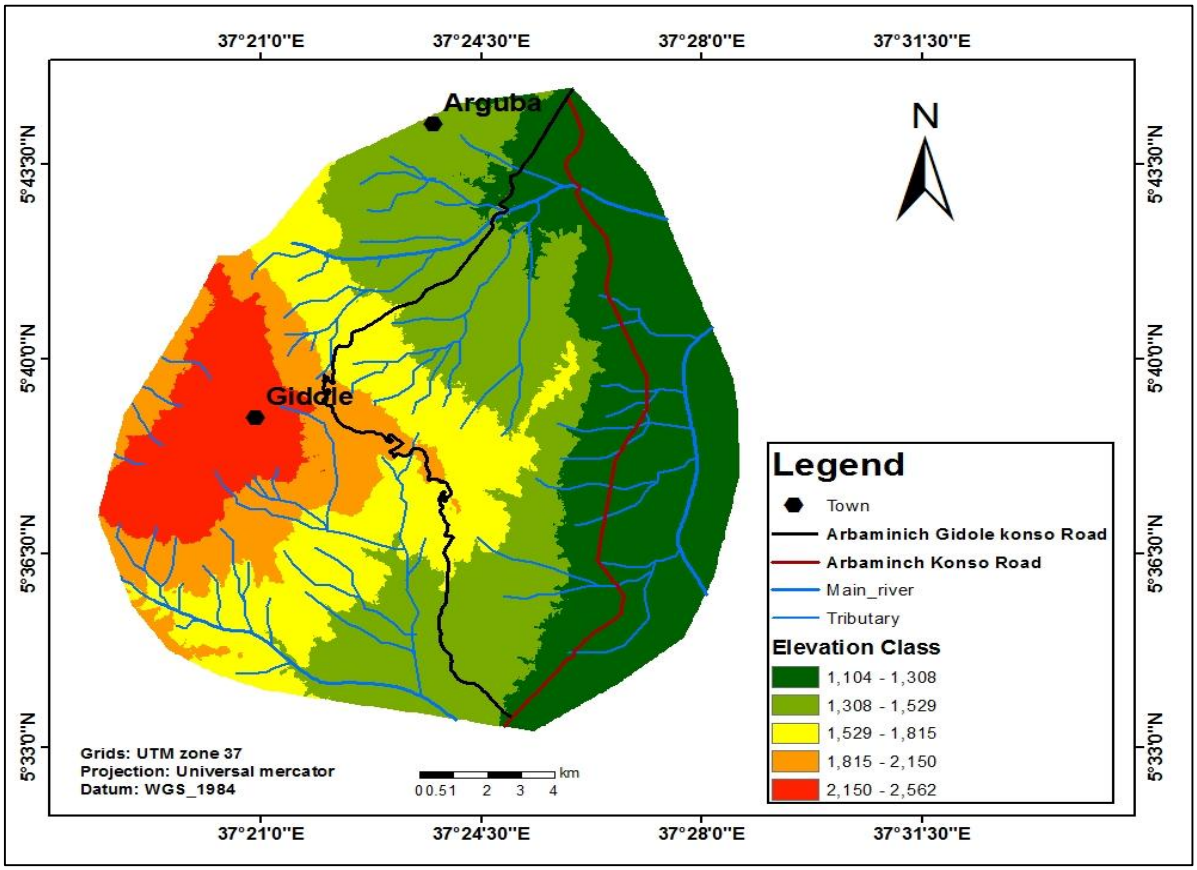

Fig.5.1 Elevation map

5.2.1.2 Slope angle

Slope angle is one of the major factors in landslide hazard. Slope inclination has direct effect on landslide process because the driving force of mass movement increases with increasing slope; therefore it is frequently used in landslide zonation map (Ayalew and Yamagishi, 2004; Ayalew *et al.*, 2005). As the slope angle increases, shear stress in soil or other un-consolidated material generally increases. Gentle slopes are expected to have a low frequency of landslides because they possess lower shear stresses associated with low gradients (Raghuvanshi *et al*., 2015; Ahmed, 2009).

Slope map was derived from SRTM DEM in a resolution of 30 m, accordingly, the slope angle in the study area ranges from 0^o to 60^o (Fig 5.2).

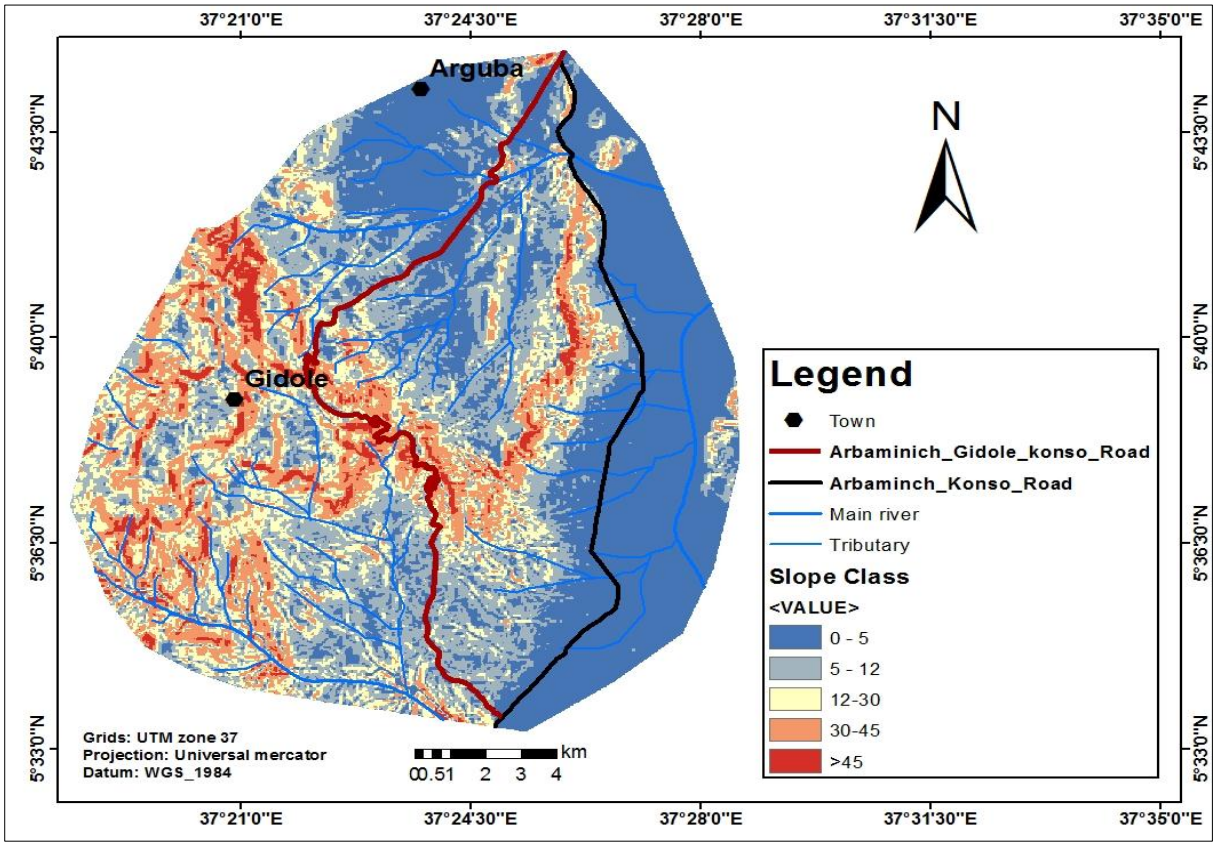

Fig. 5.2 Slope Angle map

5.2.1.3 Aspect

Aspect is defined as the direction of maximum slope of the terrain surface with reference to north (Xu*et al.,* 2012). The aspect of a slope can influence landslide initiation, because it affects moisture retention and vegetation cover, and in turn soil strength and susceptibility to landslides (Raghuvanshi *et al*., 2015).The aspect map of the study area was generated from the SRTM DEM at 30 m resolution and the aspect was classified according to the angles; Flat (-1−0^o), North (0−22.5^o), North−east (22.5−67.5^o), East(67.5−112.5^o), South−east (112.5−157.5^o), South (157.5−202.5^o), South−west (202.5−247.5^o), West (247.5−292.5^o), North−west (292.5−337.5^o) and North (337.5−360^o) (Fig 5.3).

5.2.1.4 Normalized Difference Vegetation Index (NDVI)

Vegetation provides both hydrological and mechanical effects that are beneficial to the stability of slopes, partly due to the root retaining strength and controlling of rainfall runoff movement (Chauhan *et al*. 2010).

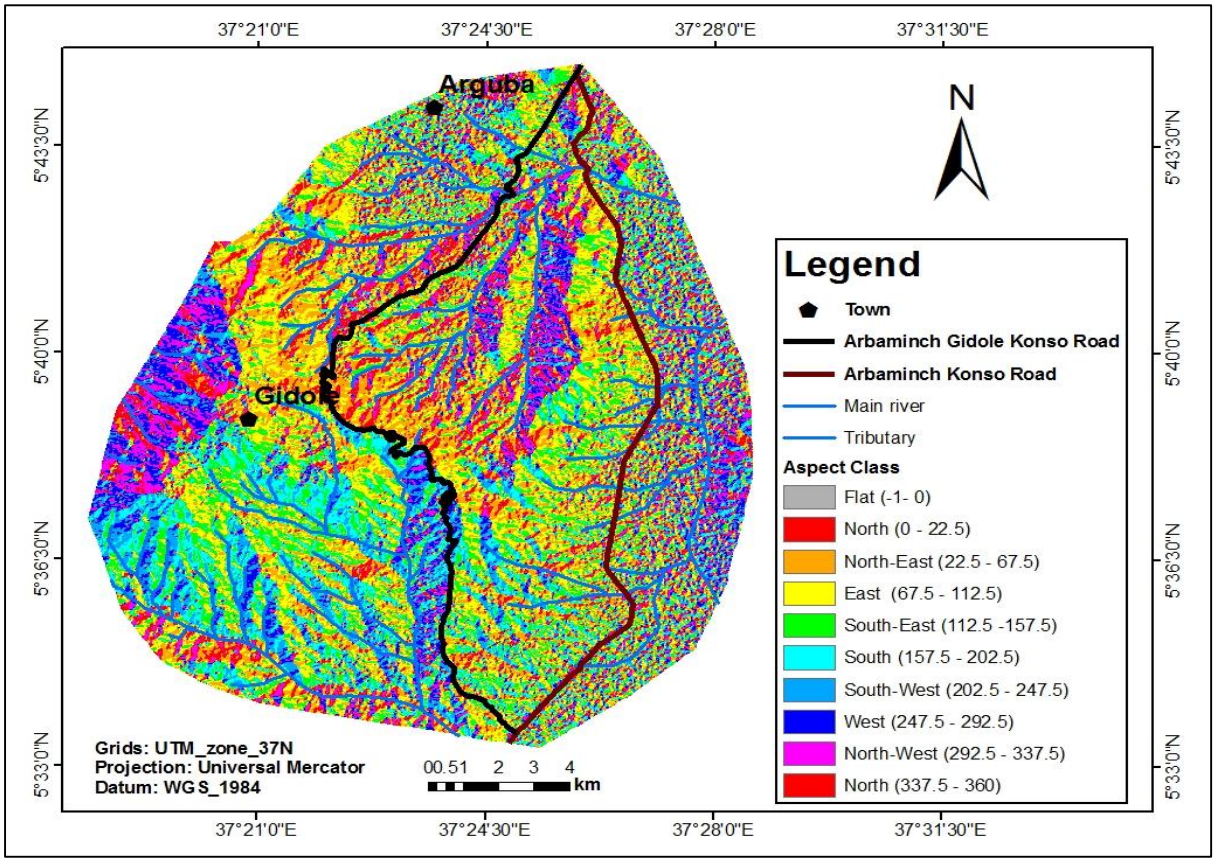

Fig. 5.3 Aspect map

The presence of dense green vegetation implies high NDVI values, due to high concentrations of chlorophyll resulting in low reflectance in red band. Sparse vegetation, on the other hand, implies low NDVI value due to less of no chlorophyll and leaves. NDVI value is calculated using (Eq. 5.1) from the Landsat 8 OLI image acquired in 2017. By using data for multispectral sensor working in the visible and NIR region of the electromagnetic spectrum, one is able to calculate the NDVI. The NDVI uses the difference of the vegetation signature between the RED (0.6−0.7μm) and NIR (0.7−1.1μm) channel (Rouse, 1974).

$$\mathrm{NDVI} = \frac{\mathrm{NIR}-\mathrm{RED}}{\mathrm{NIR}+\mathrm{RED}} \qquad (5.1)$$

The NDVI ranges from −1 to +1, as water has commonly no reflection in infrared, its NDVI is −1. The NDVI value of bare areas (rock, sand, and snow) is less than +0.1. The NDVI increases the vegetation density range +0.1 to +0.7 (Albertz and Wiggenhagen, 2009). The value of NDVI ranges from −1 to 1 where the values closer to 1 mean higher vegetation cover and values close to 0 or less than 0 means little of no vegetation cover exists (Lillsand *et al.*, 2007). As shown in (Fig 5.4), the value of NDVI in the study area ranges from −0.02 to 0.77.

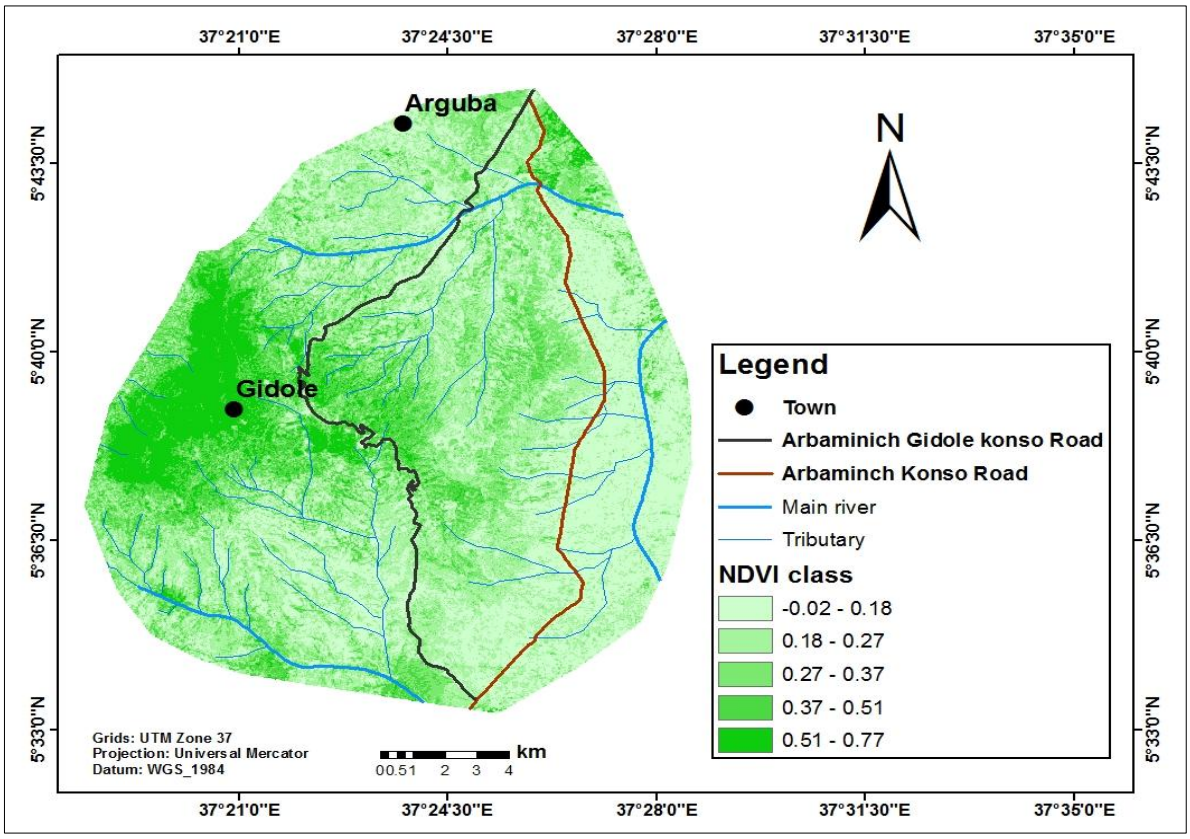

Fig. 5.4 NDVI map

5.2.1.5 Lithology

Lithology plays an essential role in the slope instability and it is correlated with the properties of the slope forming material. The erodibility of rock is highly influenced by the strength of the rock. Rocks which possess high strength are relatively more resistant to erosion (Anbalagan, 1992, Raghuvanshi *et al*., 2014). Based on the geological map at 1:25,000 scale produces by Geological Survey of Ethiopia in 2014 and data collected from the field during present study, a lithology map was prepared and converted in to GIS database. There are six categories of rock and soil types in the study area these are; basalt, pyroclastic deposit, colluvial deposit, sandstone, metamorphic rock and alluvium, sand and clay (Fig 5.5).

5.2.1.6 Land-use/land-cover

Land-use and land-cover is a key factor for landslide occurrence. Regions with dense vegetation are found to be prone to landslide than sparse vegetation, agriculture and urbanization (Raghuvanshi *et al*., 2014; Kifle Woldearegay, 2013; Anbalagan 1992; Varnes, 1987). The land-use and land-cover of the study area was classified as agricultural land, bareland, forest, built-up area and shrub/bush land (Fig. 5.6).

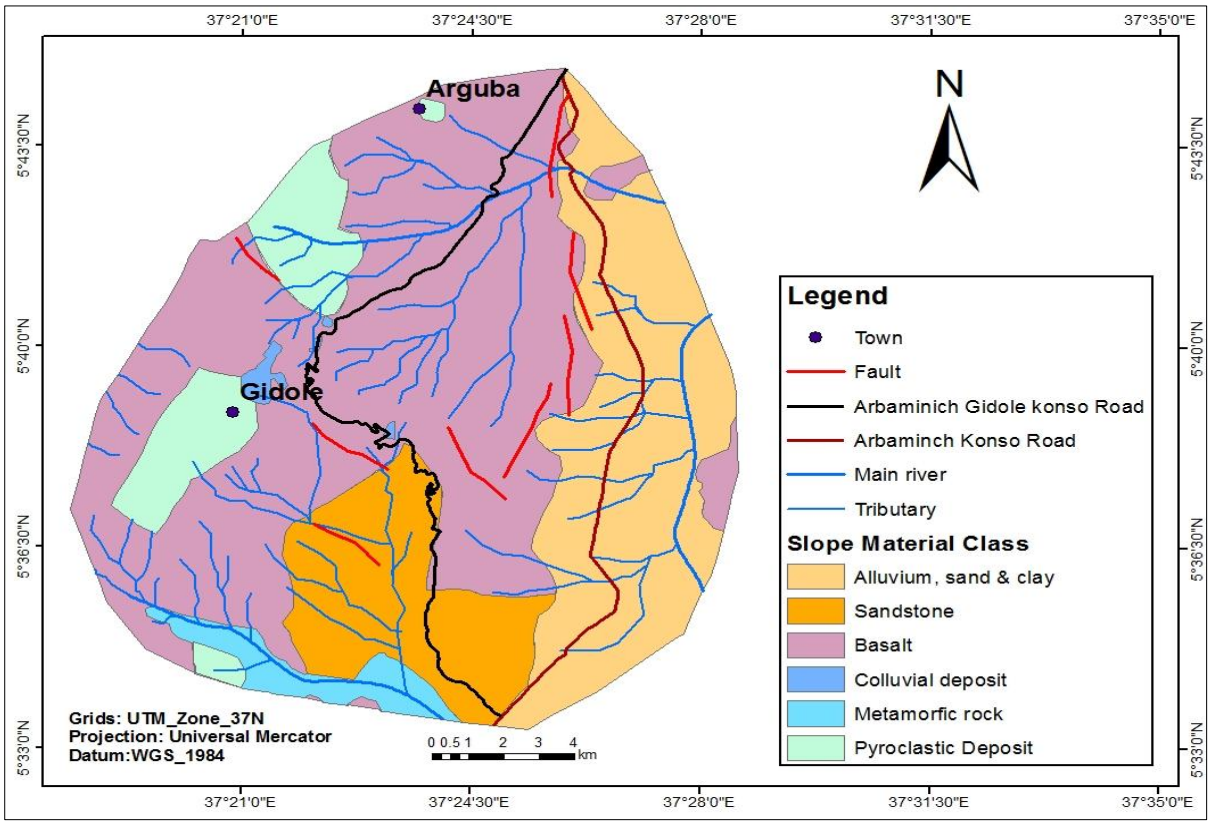

Fig. 5.5 Lithology map

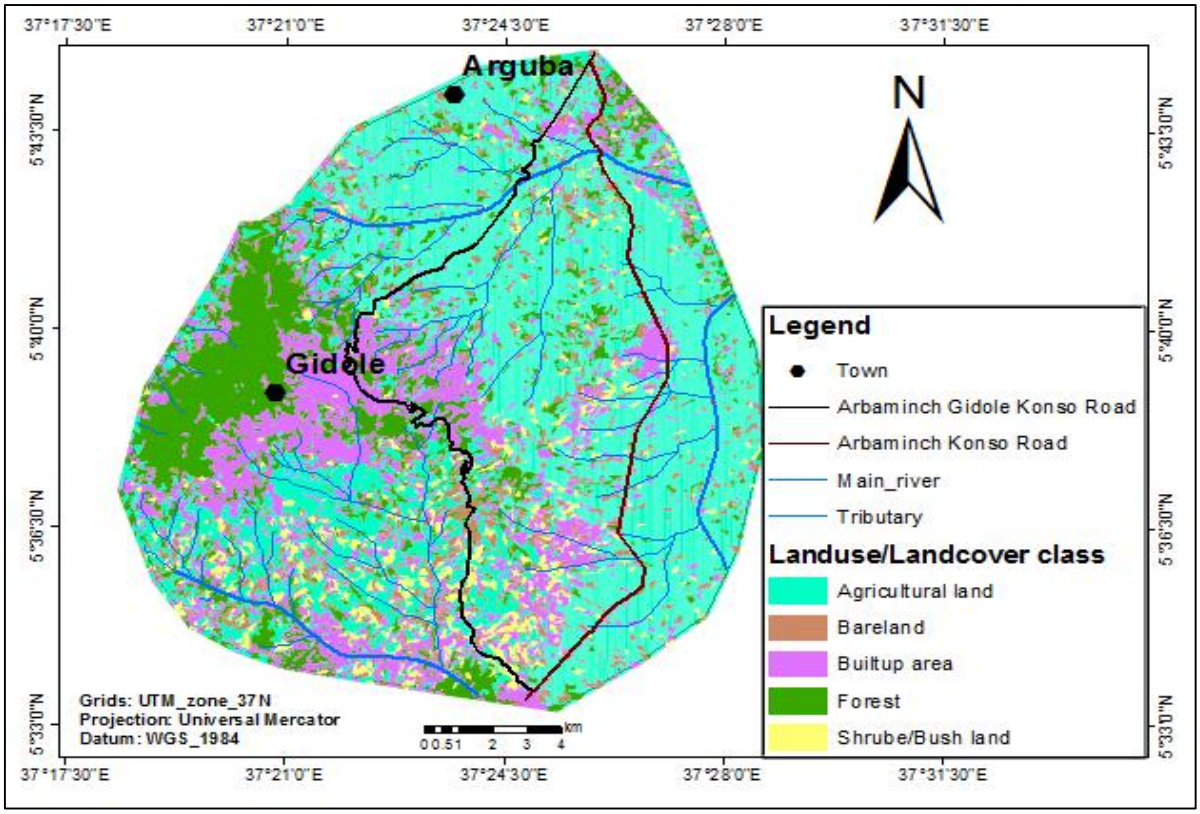

Fig. 5.6 Land-use and land-cover map

The LULC layer in the study area was classified by supervised classification method from Landsat 8 OLI 2017 satellite image at a resolution of 30m. The accuracy assessment of the classification was calculated based of field data and Google earth image. The overall accuracy of the prepared LU/LC classification is 88.64% with a kappa coefficient of 0.85.

5.3 Slope Instability analysis

5.3.1 InSAR processing dataset

To monitor the slope instability around Gidole, 7 Sentinel 1A C-Band SLC images were acquired for the study area from 2014 to 2018 by the EO satellite from the European Space Agency and were used for the analysis. Sentinel 1A image of 03 Dec 2014 is chosen as the master image based on minimizing perpendicular baseline. SAR satellites orbit the Earth at an altitude of about 700 km and revisit every location on Earth after a specific time. The time period between two successive visits the repeat cycle is called Temporal Baseline. However, the satellite may not be in the exact same location again during acquisition of the next radar image due to limitation in orbit control. The distance between two acquisition spots perpendicular to the satellite viewing direction is known as Perpendicular Baseline (Hooper, 2006). The dataset is presented in (Table 5.2) along with the perpendicular baseline length with respect to master image. The data were processed using the time-series approach of Persistent Scattered and finally done the time-series analysis to derive a two-dimensional Line-of-Sight (LOS) time-series and displacement map of surface deformation on the slope.

Table 5.2 Detail Radar image acquisition

No.	Acquisition date	Master /Slave	Polarization	Sensor mode	Product type	Passes	Orbit	Bperp (m)	Btemp (days)	Source
1	03 Dec 2014	Master	VV	IW	SLC	Descending	3549	0	0	European space agency https://scihub.copernicus.eu
2	13 Feb 2015	Slave	VV	IW	SLC	Descending	4599	119.11	72	European space agency https://scihub.copernicus.eu
3	09 Mar 2015	Slave	VV	IW	SLC	Descending	4949	44.14	96	European space agency https://scihub.copernicus.eu
4	13 Jun 2015	Slave	VV	IW	SLC	Descending	6349	71.65	192	European space agency https://scihub.copernicus.eu
5	14 Feb 2017	Slave	VV	IW	SLC	Descending	15274	6.11	804	European space agency https://scihub.copernicus.eu
6	21 May 2017	Slave	VV	IW	SLC	Descending	16674	14.71	900	European space agency https://scihub.copernicus.eu
7	09 Feb 2018	Slave	VV	IW	SLC	Descending	20524	12.03	1164	European space agency https://scihub.copernicus.eu

Sentinel 1 can collect SAR images in different modes. Interfrometric wide-Swath (IW) is the main operational mode over land, which is suitable for interfrometric application through burst synchronization. In this mode, the data covers a swath of 250km with a spectral resolution of $5\times20m^2$ in range and azimuth direction and offers the data products in single

(HH(Horizontal Transmit and Horizontal receive)/VV(Vertical transmit and Vertical receive)) or (HH+VV/ VV+VH(Vertical transmit and Horizontal receive) polarization (Torres *et al.,* 2012). To produce such a large coverage from a single acquisition in space, the SAR data in IW mode is acquired using the Terrain Observation with Progressive Scan (TOPS) operation (Zan and Guarnieri, 2006). A TOPS SAR image consists of three sub-swaths and each sub-swath is formed from several slightly overlapping subsets called bursts. Images for all bursts in all sub-swaths of an IW SLC product are re-sampled to a common pixel spacing grid in range and azimuth. This process is called TOPS SAR deburst. After co-registration of Sentinel 1 SLC image pairs, we can produce the interfromertic phase.

5.3.2 Interfrogram Generation

The interfrogram generation for PS-InSAR processing was done using a single master image which involves co-registration, resampling and complex multiplications of the master with all the slave images. The master SAR image is Dec 2014. The master image acquisition has been chosen based on stack coherence in SNAP Desktop software. The aim of the master selection using stack coherence is to minimize the total decorrelation of all the interfrograms. Alongside, this approach is able to maximize the total correlation of the interfrometric stack based on the perpendicular baseline, temporal baseline and the mean Doppler centroid frequency difference (Hooper, 2006).

The interfrometric phase which is phase difference between master and slave image is calculated as:

$$\Delta\varphi_{interfrogram} = \Delta\varphi_{Def} + \Delta\varphi_{topo} + \Delta\varphi_{Curv} + \Delta\varphi_{atm} + \Delta\varphi_{noise} \quad (5.2)$$

Where $\Delta\varphi_{interfrogram}$is the interfrogram is the interfrometric phase, $\Delta\varphi_{Def}$is the phase component due to deformation, $\Delta\varphi_{topo}$is associated with area topography, $\Delta\varphi_{Curv}$ is the phase component due to Earth curvature, $\Delta\varphi_{atm}$ is atmospheric phase resulting from the different atmospheric delay at the different acquisition times, and $\Delta\varphi_{noise}$ is noise term primarily due to the decorrelation (Zebker and Goldstein, 1986). The interfrogram phase is the sum of contribution from several factors. In order to estimate the deformation, all other components have to be estimated and subtracted from the interfrometric phase. DEM and precise orbit information are used to model and remove phase contributions due to Earth curvature and topography.

5.3.3 StaMPS approach Persistent scattered selection

Once the interfrograms were generated and the topographic phase was removed using DEM to convert the interfrograms in to differential interfrograms which were suitable for PS processing, the phase stability test was applied to obtain a set of phase stable pixels. In PS interferometry, the signal return from the dominant scattered in the resolution element. StaMPS use amplitude Dispersion value which is the ratio of the standard deviation and the mean of the amplitude value to select a subset of pixels that includes almost all of the PS pixels in the dataset. The pixels are selected on the bases of amplitude stability, in which those pixels which have a value of the amplitude dispersion index with the threshold are selected as initial PS candidates(Hooper, 2007). The data input for PS-InSAR processing in StaMPS is a stack of differential interfrograms coregistered to a selected master image. In this study, the threshold value used for amplitude dispersion was taken as 0.42. The parameter used for StaMPS based PS-InSAR processing is shown in (Table 5.3).

Table 5.3 Parameters used for PS candidate selection

No	Parameter	Value
1	Amplitude Dispersion threshold	0.42
2	Number of patches in range	1
3	Number of patches in Azimuth	1
4	Overlapping pixel between patches in range	50
5	Overlapping pixels between patches in azimuth	200

The first PS-InSAR observation is the double difference between mater and slave for two nearby PS (Hanssen, 2004). The double difference is both a temporal and a spatial difference. This implies that StaMPS also requires a spatial and temporal reference one acquisition time i.e master image and one reference PersistentScattered.The PS-InSAR algorithm gives a temporal evolution of the landslide in Gidole over 4 years using multiple SAR image acquisition. Setting the amplitude dispersion higher in the processing parameter can increase the number of initial PS candidates. The selected PS pixels are in wrapped between $-\pi$ and $+\pi$ (Fig 5.7), phase unwrapping therefore implemented in order to obtain continuous deformation phase value. In this study, 3D phase unwrapping has been performed, two spatial and one temporal. The temporal phase difference for each PS pixel are calculated and then unwrapped spatially from reference PS pixels using an iterative least square method. PS pixel is also filter using Goldstein phase filter before performing unwrapping (Fig. 5.8), high-pass filtering can be applied to the unwrapped data in order to remove the remaining look angle,

atmosphere and orbit errors (SCLA). By subtracting SCLA errors from PS pixels, it leaves only phase data due to deformation.

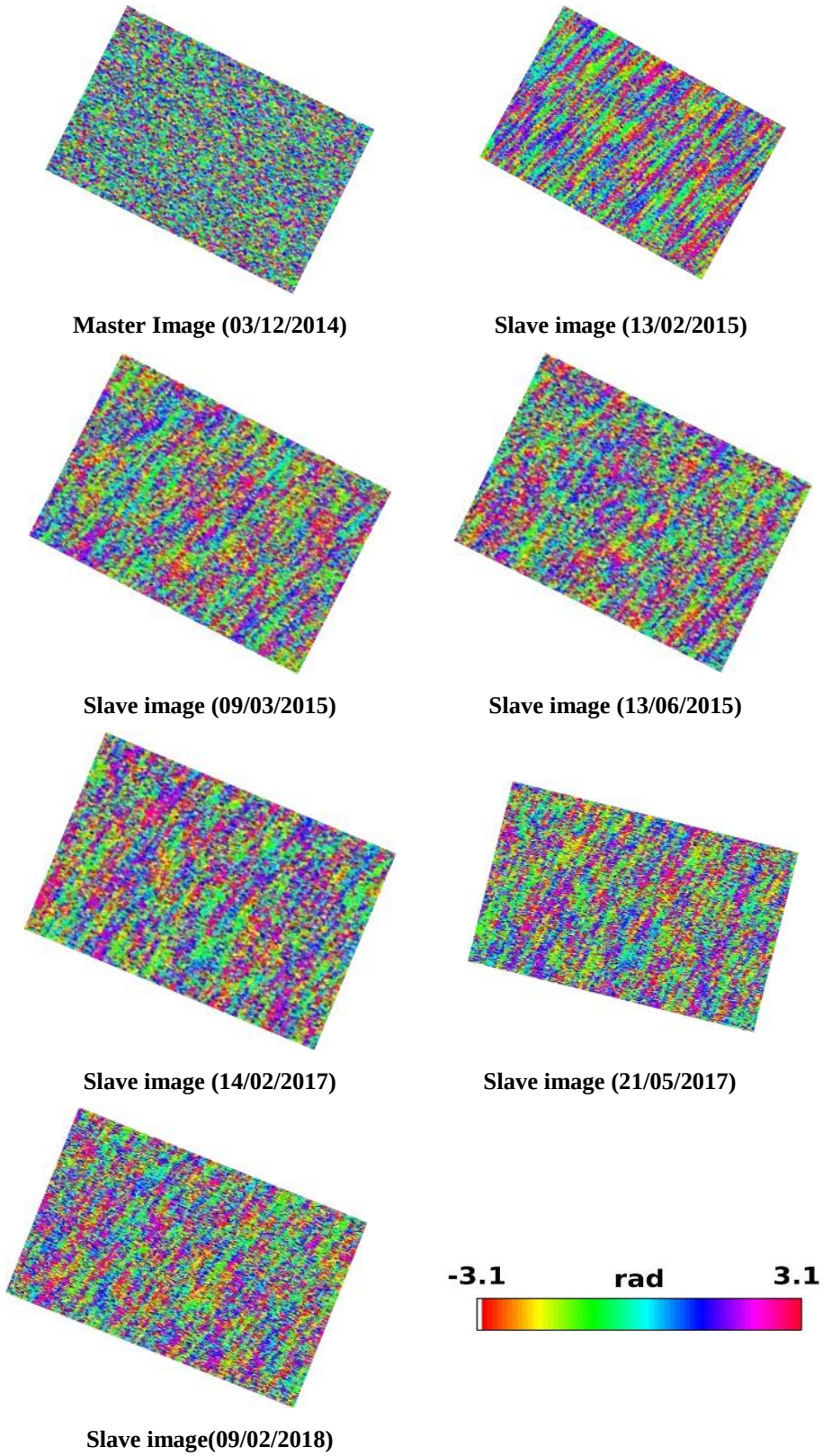

Fig. 5.7 Wrapped Interfrograms with master image during 2014−2018

Master Image (03/12/2014)

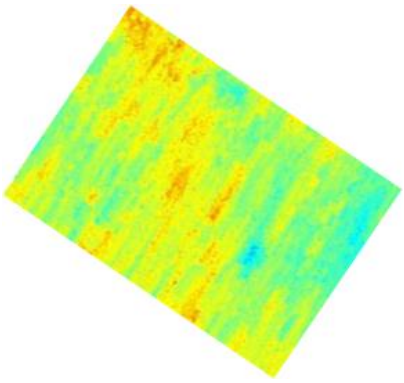

Slave image (13/02/2015)

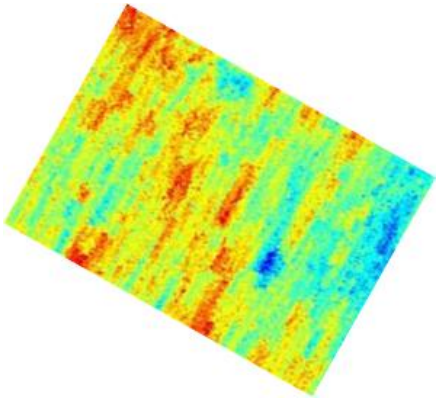

Slave image (09/03/2015)

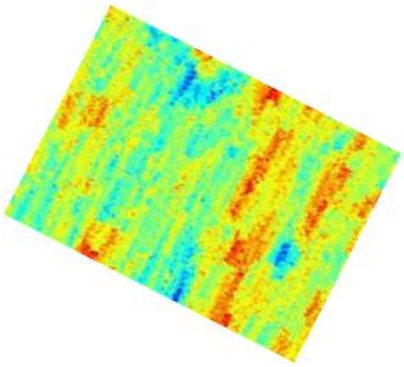

Slave image (13/06/2015)

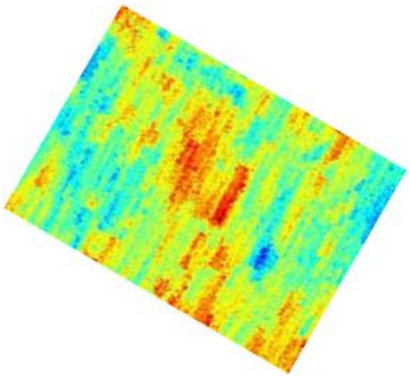

Slave image (14/02/2017)

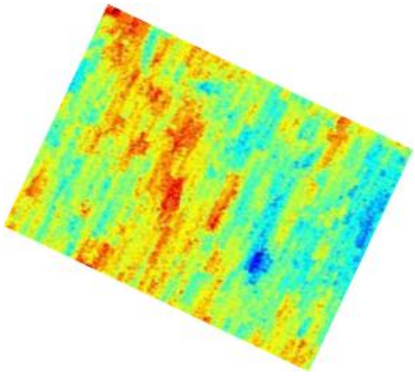

Slave image (21/05/2017)

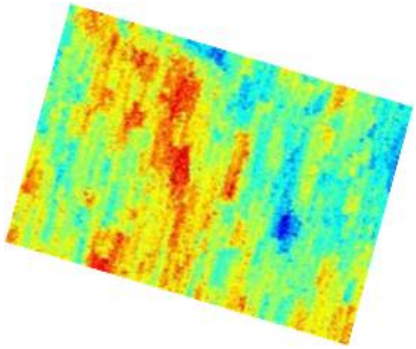

Slave image(09/02/2018)

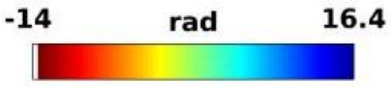

Fig. 5.8 Unwrapped Interfrograms with Master Image

Wrapped interfrograms from descending orbit data acquire over Gidole landslide. The master acquisition data is 13 Feburary 2014. Each color fringe represents $-\pi$ and π mm of displacement in the LOS After phase unwrapping, high-pass filtering is applied in order to remove the remaining errors. Finally, the displacement can then be estimated using the phase values of the individual PS pixels. A Line of Sight (LOS) velocity map is generated as an output of the StaMPS method.

*****

CHAPTER SIX RESULTS AND DISCUSSION

6.1 Landslide Inventory mapping

Landslide inventory map is essential and key starting point for studying the relationship among landslide and conditioning factors (Raghuvanshi et al., 2015). Out of total 39 number of landslides identified and mapped in the study area, 37 (94.7%) landslides are found in the western and southern parts of the Arbaminch-Gidole-Konso road project (Fig 6.1). This clearly indicates that along the side of the main road the risk of landslide occurrence is increased due to excavation of toe support or the sides of the slope. This has further caused reactivation of the old landslides and formation of new landslides.

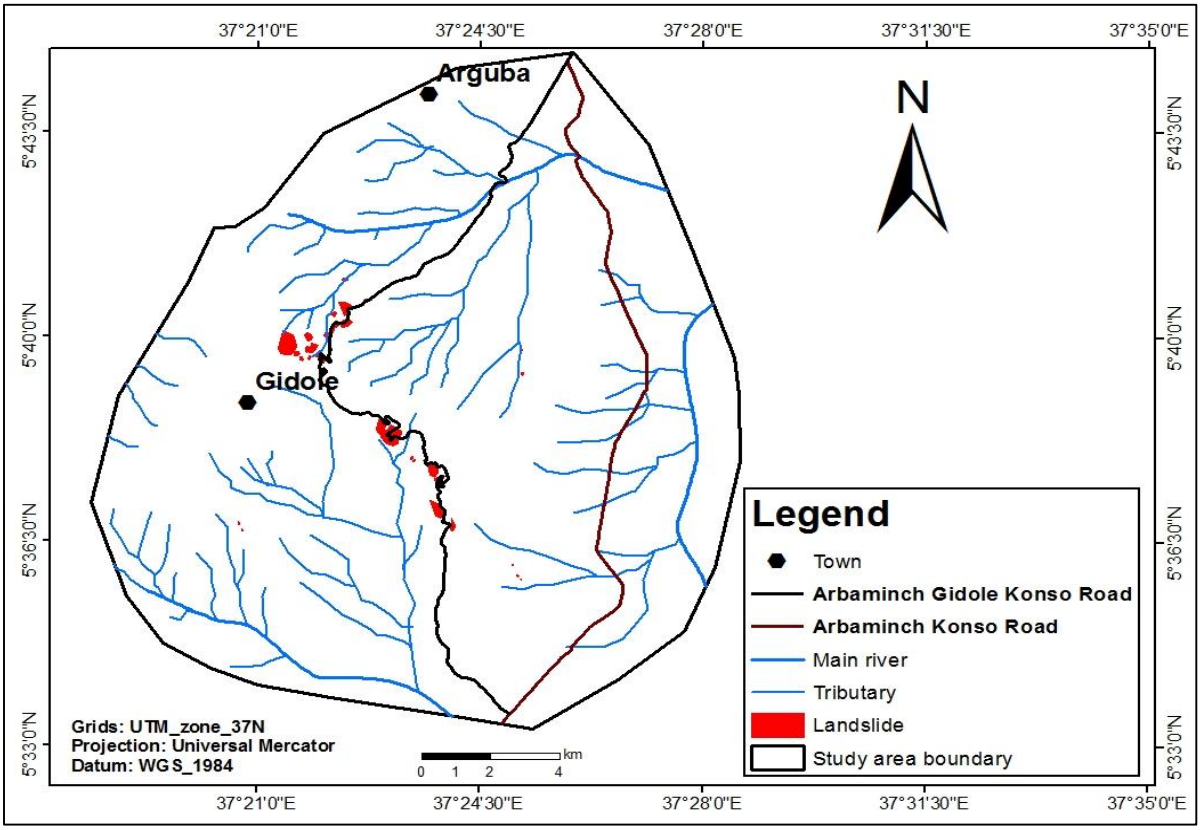

Fig. 6.1 Landslide Inventory map

6.2 Landslide hazard zonation

6.2.1 Triggering factors influence on landslides

At the beginning, in the present study, through field work and review of previous works, the six factors including aspect, slope, elevation, lithology, NDVI and LULC were recognized as primary triggering factors for landslide occurrence (Anbalagan, 1992; Raghuvanshi et al., 2014; Tilahun Hamza and Raghuvanshi, 2017).

6.2.1.1 Aspect

In this study slope aspect was divided at every 45°. Thus, there are nine intervals. According to the result shown in Table 6.1 it can clearly be seen that landslide occurrence in the slopes inclined towards South, Southwest, North and Northeast show 'information values' (IV) 0.09, 0.19, 0.08 and 0.05, respectively. Further, from the landslide inventory data it was observed that South facing slopes covered the highest percentage of landslides (42.7%) followed by north facing slopes (32.8%). Relatively less number of landslides occurred in other aspect classes. No landslides were observed to occur in flat aspect class.

Table 6.1 Landslide distribution according to Aspect class

Value	Class	Factor class pixel	Pixels %	Landslide with factor class	Landslide %	Conditional Probability	Prior Probability	Weight of factor class	IV
1	Flat	112	0.0	0	0	0	0	0	0
2	North	19882	6.9	96	8.3	0.0048	0.0040	1.21	0.08
3	North East	50928	17.7	229	19.8	0.0045	0.0040	1.12	0.05
4	North west	22724	7.9	54	4.7	0.0024	0.0040	0.59	-0.23
5	South	34606	12.0	172	14.9	0.0050	0.0040	1.24	0.09
6	South East	46973	16.4	145	12.6	0.0031	0.0040	0.77	-0.11
7	South West	28221	9.8	175	15.2	0.0062	0.0040	1.55	0.19
8	West	25921	9.0	84	7.3	0.0032	0.0040	0.81	-0.09
9	East	57910	20.2	199	17.2	0.0034	0.0040	0.86	-0.07

6.2.1.2 Slope

The study area was classified in to five slope classes i.e. 0 - 5^o (21.7% of the study area), 5-12^o (41.7% of the study area), 12 - 30^o (33.3% of the study area), 30 - 45^o (3.2% of the study area) and >45^o (0.1% of the study area). According to (Table 6.2), 6.5%, 30.9%, 56.5%, and 6.5% of landslide occurred in 0 - 5^o, 5 - 12^o, 12 - 30^o and 30 - 45^o, respectively. The slope classes 0 - 5^o, 5 -12^o, 12 - 30^o and 30 - 45^o show 'information value' (IV) of − 0.52, − 0.13, 0.23 and 0.28, respectively.

Further, slope angle classes 0 - 5^o, 5 - 12^o and > 45^o show low information value (IV), this indicate a low probability of landslide occurrence within these slope classes. However, the slope classes 12 - 30^o and 30 - 45^o show highest probability of landslide occurrence with information value (IV) 0.23 and 0.28, respectively. No landslides occurred in slope class >45^o. The relation between landslide occurrence and slope angle shows that most of the landslides were observed in slopes having slope angle ranging from 12^o to 45^o (Table 6.2).

Table 6.2 Landslide distribution according to slope Angle class

Value	Class (º)	Factor class pixel	Pixels %	Landslide with factor class	Landslide %	Conditional probability	Prior probability	Weight of factor class	IV
1	0−5	66683	21.7	79	6.5	0.0012	0.0039	0.30	-0.52
2	5−12	128049	41.7	374	30.9	0.0029	0.0039	0.74	-0.13
3	12−30	102176	33.3	684	56.5	0.0067	0.0039	1.70	0.23
4	30−45	9771	3.2	73	6.0	0.0075	0.0039	1.90	0.28
5	>45	428	0.1	0	0	0	0.0039	0	0

6.2.1.3 Elevation

Elevation is a factor frequently utilized in landslide hazard assessment (Raghuvanshi et al., 2014; Tilahun Hamza and Raghuvanshi, 2017). According to the results shown in (Table 6.3), 1815−2150 m and 1529−1815 m classes of elevation have 58.2% and 40.5% of historic landslide occurrence and these two elevation classes have the highest information value (IV) of 0.71 and 0.31, respectively. From these figures it may be realized that the information value generally increase with the increase in elevation. No landslides occurred in elevation class 1104−1308 m and 1308−1529 m, respectively

Table 6.3 Landslide distribution according to Elevation class

Value	Class	Factor class pixel	Pixels %	Landslide with factor class	Landslide %	Conditional probability	prior probability	weight of factor class	IV
1	1104−1308	88574	28.8	0	0	0	0.0040	0	0
2	1308−1529	91994	30	10	0.8	0.00011	0.0040	0.03	-1.57
3	1529−1815	61364	20	500	40.5	0.00815	0.0040	2.04	0.31
4	1815−2150	35003	11.4	719	58.2	0.02054	0.0040	5.13	0.71
5	2150−2562	30172	9.8	0	0	0	0.0040	0	0

6.2.1.4 Normalized deference vegetation index

Vegetation in general improves the stability of the slope (Anbalagan, 1992; Raghuvanshi et al., 2014). The NDVI value in general reflects on the vegetation coverage rate and the health of the study area. The results presented in Tables 6.4 clearly indicates that higher information values (IV) (0.13 to 0.29) are distributed for NDVI classes falling between 0.02 to 0.37, which generally corresponds to built-up area, agricultural land and shrub/bush lands. As NDVI becomes higher (>0.37) probability of occurrence of landslide is lower. From this it can be realized that as the NDVI increase the Information value (IV) in general decreases.

The relation between landslide occurrence and NDVI clearly showed that most of the landslides occurred in the area were the NDVI values were low, particularly NDVI value less tha 0.29.

Table 6.4 Landslide distribution according to NDVI class

Value	Class	Factor class pixel	Pixels %	Landslide with factor class	Landslide %	Conditional probability	Prior probability	Weight of factor class	IV
1	-0.02−0.18	9952	14.1	241	19.5	0.0242	0.0175	1.38	0.14
2	0.18−0.27	10367	14.7	246	19.9	0.0237	0.0175	1.35	0.13
3	0.27−0.37	9596	13.6	330	26.6	0.0344	0.0175	1.96	0.29
4	0.37−0.51	20879	29.5	332	26.8	0.0159	0.0175	0.91	-0.04
5	0.51−0.77	19875	28.1	90	7.3	0.0045	0.0175	0.26	-0.59

6.2.1.5 Lithology

Table 6.5 presents the landslide occurrence computed for the six classes of the lithology. The information value (IV) as computed for colluvial deposit, Basal sandstone and pyroclastic deposit are 0.89, 0.30 and 0.19, respectively which in general demonstrates higher number of landslides in the area. Particularly, colluvial deposit which dominates in the western part of the study area show significant slope instability problems and have highest IV value of 0.89. Further, metamorphic rock and alluvium sand and clay deposits also demonstrate a higher information value of 0.61 and 0.47, respectively.

Table 6.5 Landslide distribution according to lithology class

Value	Class	Factor class pixel	Pixels %	Landslide with factor class	Landslide %	Conditional probability	Prior probability	Weight of factor class	IV
1	Pyroclastic Deposit	3915	7.7	134	11.9	0.0342	0.0223	1.53	0.19
2	Basal sandstone	4126	8.2	183	16.2	0.0444	0.0223	1.99	0.30
3	Basalt	27261	53.9	620	54.9	0.0227	0.0223	1.02	0.01
4	Colluvial deposit	1123	2.2	193	17.1	0.1719	0.0223	7.69	0.89
5	Metamorphic rock	1844	3.6	10	0.9	0.0054	0.0223	0.24	-0.61
6	Alluvium, sand & clay	12310	24.3	94	8.3	0.0076	0.0223	0.34	0.47

6.2.1.6 Land-use and land-cover

The landuse and landcover of the study area was classified as: forest, built-up area, bare-land, agricultural land and bush/shrub land. Perusal of results in Table 6.6 shows that in

agricultural land, which covers 36.7% of the total study area, the total area covered within landslides is 51.92% and the information value as computed is 0.15. Thus, agricultural land in the study area shows highest probability for landslide occurrence in the study area. This is followed by bare land which covers 10.7% of the total study area, the total area covered within landslides is 13.78% and the information value as computed is 0.11. This class also shows reasonable probability for landslide occurrence. Moreover, Forest, Built-up area and bush land which covers 21.41, 23.43 and 7.75% of the study area show least probability for landslide occurrence as the information values for these classes are -0.3, -0.2 and 0.05, respectively.

Table 6.6 Landslide distribution according to land use-land covers class

Value	Class	Factor class pixel	Pixels %	Landslide with factor class	Landslide %	Conditional probability	Prior probability	Weight of factor class	IV
1	Forest	12520	21.42	119	10.86	0.0095	0.0187	0.51	-0.30
2	Built-up area	13698	23.43	161	14.69	0.0118	0.0187	0.63	-0.20
3	Bareland	6254	10.70	151	13.78	0.0241	0.0187	1.29	0.11
4	Agricultural land	21453	36.70	569	51.92	0.0265	0.0187	1.41	0.15
5	Bush land	4529	7.75	96	8.76	0.0212	0.0187	1.13	0.05

6.2.1.7 Prominent classes among various causative factors classes

The landslide is a complex process and various causative factors contribute in its occurrence. In the present study six causative factors were considered namely; aspect, slope, elevation, NDVI, lithology and land use/ landcover. From the past landslide data relational statistical correlation with various causative factors was established and prominence of various causative factor classes was worked out with the help of information value. Table 6.7 present the highest information value in respective factor class. A perusal of Table 6.7 clearly shows that the slopes which are trending toward Southwest having slope angle between 30^{o} to 45^{o} are more prone for landslide hazard. Similarly, slope falling within elevation class 1815 to 2150m are more susceptible for instability. Also, landslide probability within colluvial deposits and agricultural land is high.

6.3 Landslide hazard Evaluation and Zonation

For landslide hazard evaluation during the present study spatial relationship between the occurrence of landslides and each landslide causative factor class was derived. The distributions of landslide occurrence over each factor maps have been obtained using the

information value model. The information values are assigned to each class to obtain weighted factor map.

Table 6.7 Highest Information value Classs

Causative Factors	Class	Information Value
Aspect	South west	0.19
Slope angle	30°−45°	0.28
Elevation	1815−2150m	0.71
NDVI	0.27−0.37	0.29
Lithology	Colluvial deposit	0.89
Land use/land cover	Agricultural land	0.15

Each factor maps were summed up using raster calculator to calculate the landslide susceptibility index for each pixel. The relation analysis is the information value of the area where landslides occurred to the total area, if the value is higher relative to other classes, it shows a higher correlation; if lower, it indicates a lower correlation. Classification determines the spatial distribution of landslide on equal area classes. Therefore, the pixels of landslide susceptibility values were divided in to five classes very high hazard (VHH), high hazard (HH), moderate hazard (MHH), low hazard (LH) and very low hazard (VLH) zone by quintile (equal area) classification shown in (Fig 6.2).

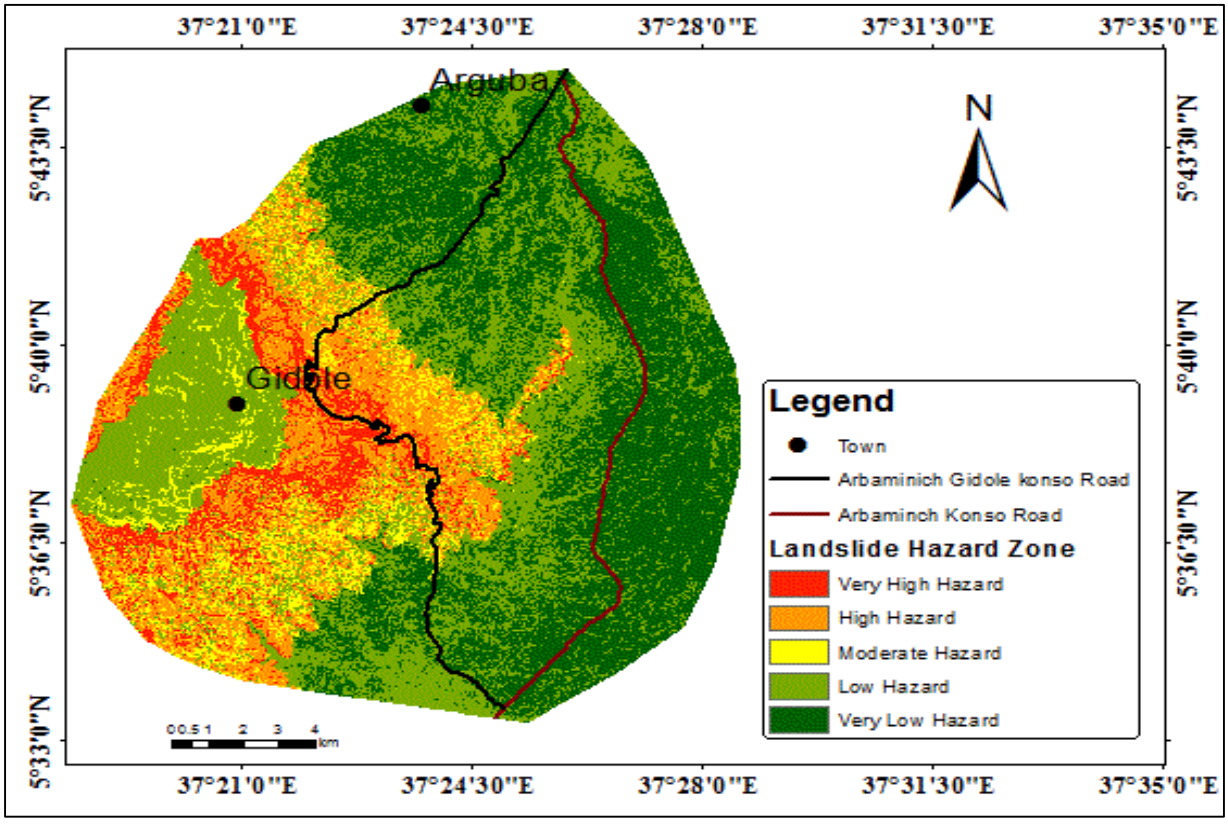

Fig. 6.2 Landslide Hazard Zone map

In the present study main factors that are possibly responsible for landslide occurrence are lithology, elevation, slope angle, aspects, NDVI and LU/LC. Combination of various factor classes might have resulted into landslide in the area. The evaluation of these factors based on statistical correlation with the past landslides formed the basis to delineate the study area into various landslide potential classes. The landslide hazard zonation map thus prepared (Fig 6.2, Table 6.8) clearly indicates that the majority of the study area 78.38km^2 (36.3%) fall within very low hazard (VLH) zone and 72.85km^2 (34.2%) of the area fall within low hazard (LH) zone. Perusal of results further shows that 12.78 km^2 (6.6%), 32.72 km^2 (15.4%) and 15.89 km^2 (7.5%) of the area falls into very high hazard (VHH), high hazard (HH) and moderate hazard (MH), respectively.

Table 6.8 Probability of different landslide hazard zones

No	Landslide hazard zone	Value	Class Pixel	Area %	Area (km^2)
1	Very high	1.26 −0.64	20325	6.6	12.78
2	High	0.64 −0.13	47087	15.4	32.72
3	Moderate	0.13 – 0	22888	7.5	15.89
4	Low	0 − (-0.26)	104845	34.2	72.85
5	Very low	-0.26 − (-2.37)	111390	36.3	78.38

6.4 Model validation of Landslide hazard zone map

In order to validate the LHZ map prepared during the present study overlay analysis was made with the past landslide inventory data (Fig. 6.3). The overlay analysis clearly showed that out of 39 past landslides inventory data 23(58.97%) falls in very high hazard (VHH) zone, 13(33.33%) falls in high hazard (HH) zone, 2(0.05%) falls in moderate hazard (MH) zone and 1(0.02%) falls in low hazard (LH) zone. This shows that 92.3% of the existing landslides fall in very high hazard (VHH) and high hazard (VHH) zone. Thus, it can safely be concluded that the hazard zones delineated in the present study validates with the past landslide data and the potential zone depicted can reasonably be applied for safe planning of the area.

6.5 Slope instability assessment

6.5.1 Displacement map and Time series analysis

The landslide deformations in Gidole area is analyzed by using the mean deformation velocity of PS-InSAR, these techniques can be used to observe displacement in the study area especially the area which have very high hazard and high hazard zones in the landslide hazard zonation map. Time series analyses have been done using PS-InSAR techniques. PS-

InSAR processing using 6 single master interfrograms showed us a total of 165,263 PS candidates are selected based on the Dispersion Amplitude index value. The displacement located in the study area has gradually increasing starting from 15.3 mm/yr. up to -19.2 mm/yrshown in (Fig 6.4). The displacement phase derived from interfrograms is a measure for the surface displacement in the satellite's line of sight (LOS).

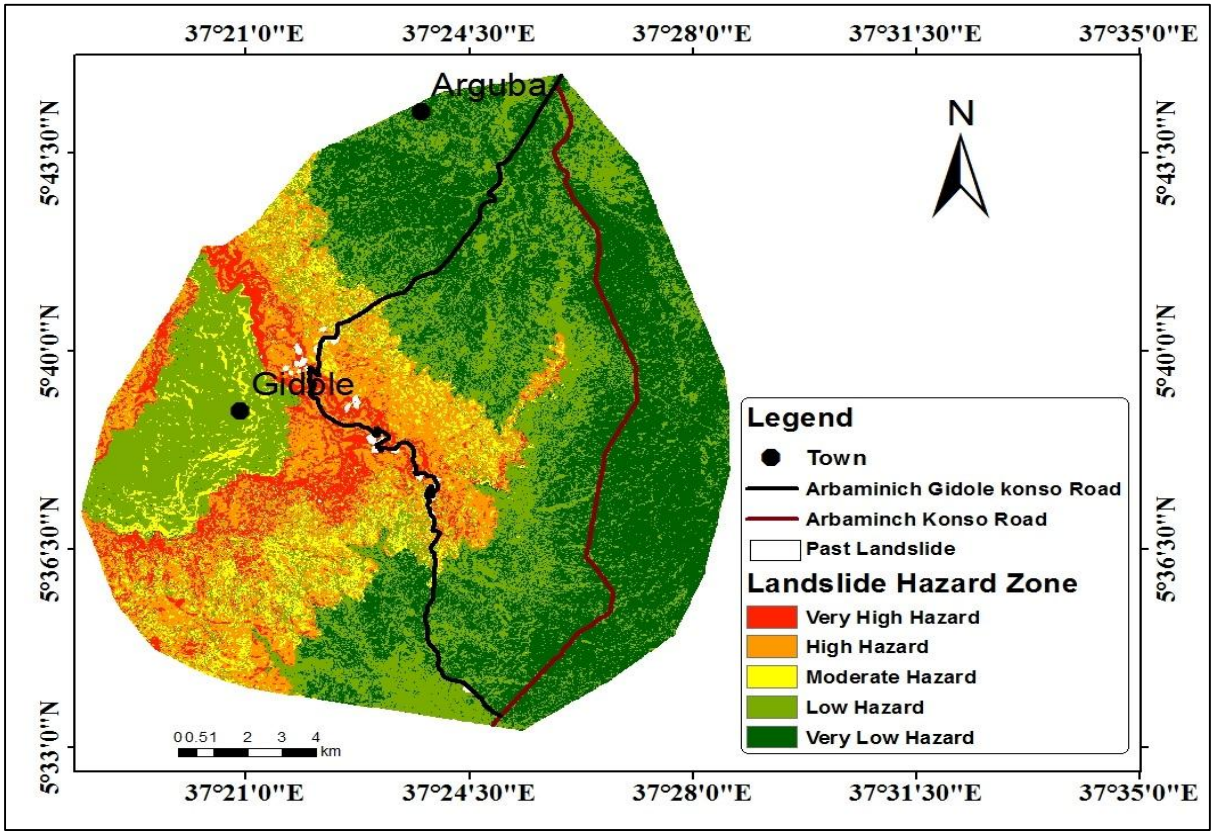

Fig. 6.3 Validation of LHZ map with past landslide data

The results in this study are represented in terms of vertical displacement that is projection of LOS displacement vertical to the vertical axis. Negative displacement indicates that the land surface is moving away from the satellite LOS continuously and the positive sign indicate the area is moving toward LOS.

To better illustrate the time evolution of surface displacement, 4 points are selected and plotted their time series (Fig 6.5). These pointes are located western, southern and central part of the study area of the sliding surface. These points are selected based on landslide inventory map. Figure 6.5 shows the time series points indicate downward movement. The magnitude of these movement ranges from 11 up to −19 mm in the analyzed period. The dynamics of the observed movement is differentiated depending on the part of the landslide area.

During four years of investigation the area involved in the Gidole landslide increased. To investigate the displacement rates we gain plotted the time series in (Fig 6.6) shows that the stack of images avagering the time series for all the parsistant scaterrer in the areas where line of sight displacements seems to be typical for landslide slope.

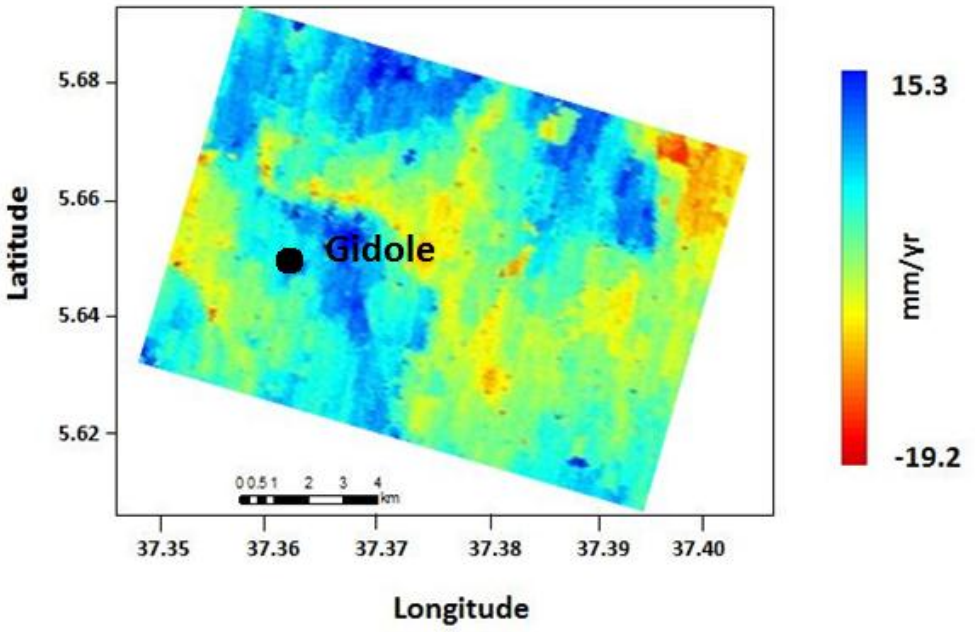

Fig. 6.4 Mean displacement velocity map during 2014−2018

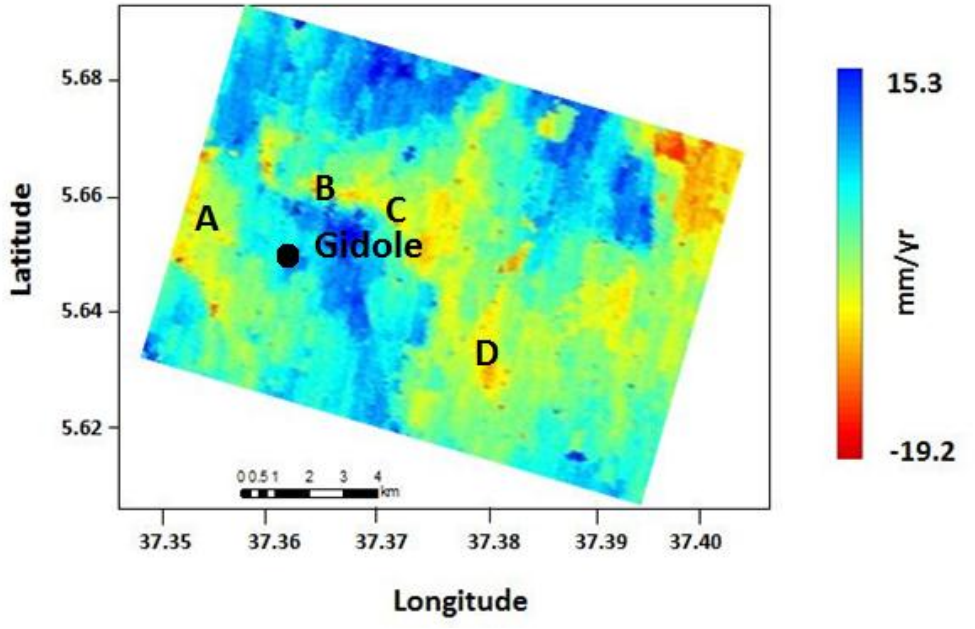

Fig. 6.5 Distribution of points in the landslide area

The present study is aimed to the fact that the process of surface displacement in the area is still active. In addition, it is observed that the change in the direction of movement to uplift in

the mid of 13/02/2015 and 09/03/2015 in all points of the time series analysis. The uplift rate is about 8-19 mm/yr. in all PS points. The analyses presented in Fig. 6.7 shows that the observed signals do correlate with the average monthly precipitation. The major slope failure in the area was reactivated in 2015 after high rainfall.

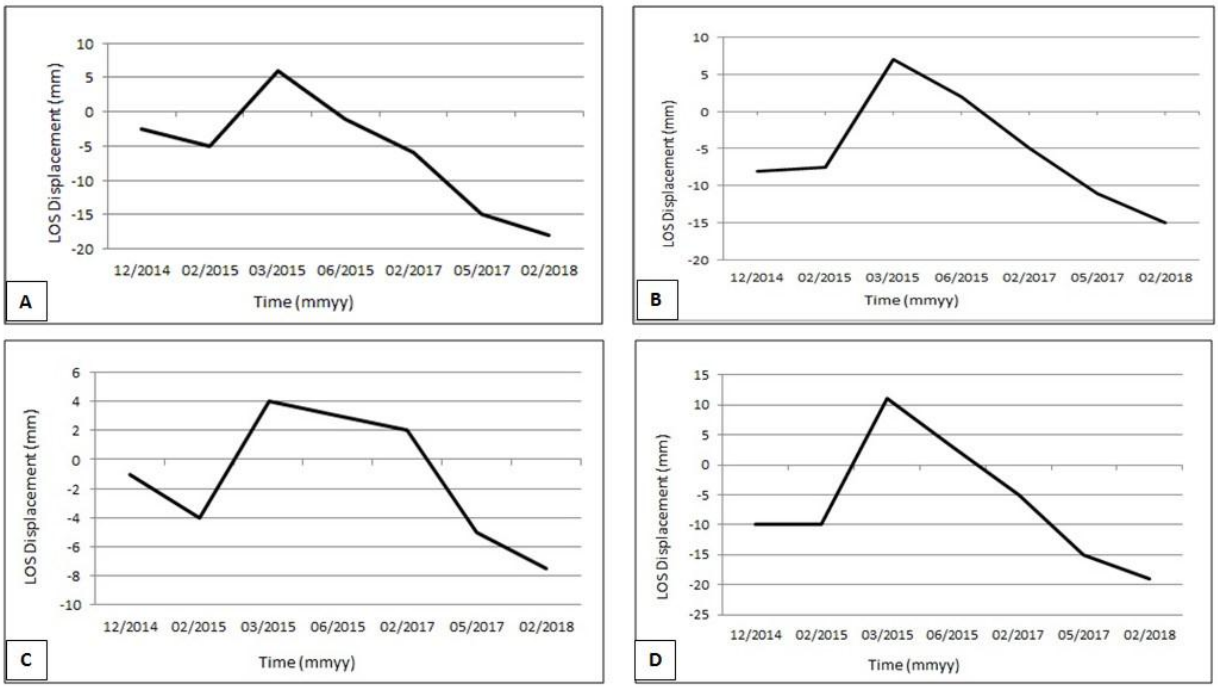

Fig. 6.6 LOS Displacement time series of the selected PS points (A,B,C,D) during 2014−2018

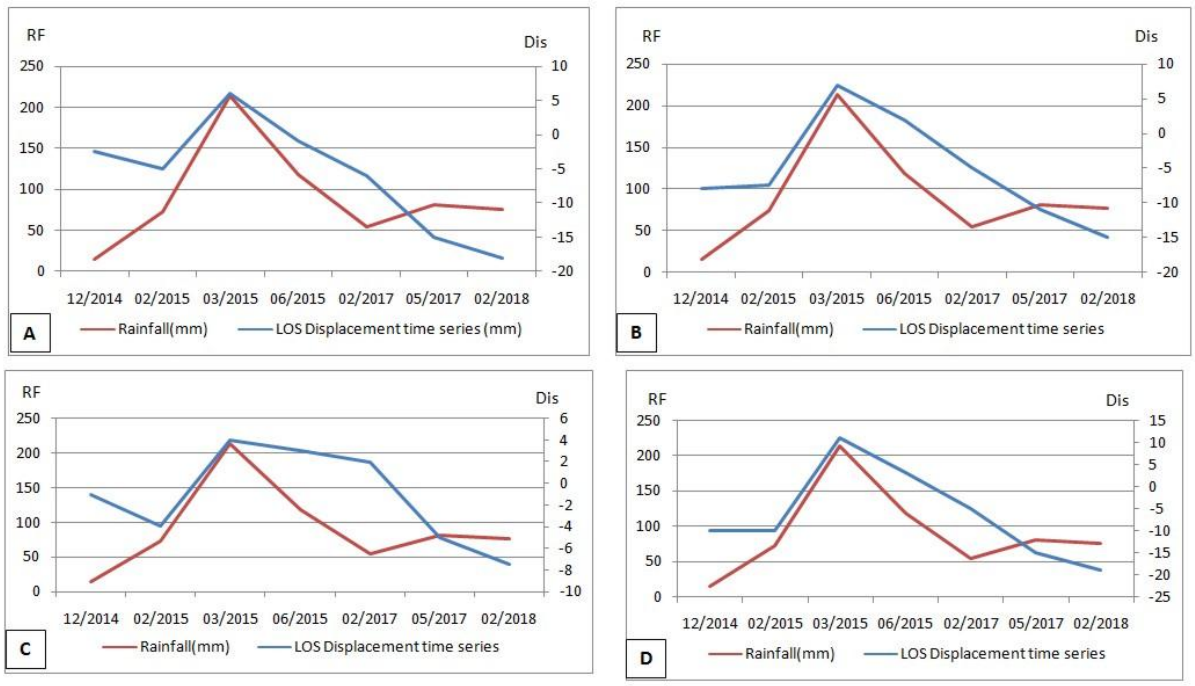

Fig. 6.7 LOS Displacement time series of the selected PS points (A, B, C, D) with rainfall

6.6 Discussion

Among the various natural hazards, landslides are the most widespread and damaging hazard. They cause loss of life and property, damage to natural resources such as vegetation, land and soil and hamper developmental projects like roads, bridges and communication lines (Gemechis Chimindi et al., 2017; Tilahun Hamza and Raghuvanshi, 2017; Raghuvanshi et al., 2015).

The results of the present study showed that the landslides were dominant in the Southwest facing slopes. This might be related to the fact that the Southwest facing slopes are more exposed to rainfall and other hydrological and hydrogeological factors are more significant in contributing for landslides. Further, aspect of the slops plays a role in controlling some microclimatic factors such as exposure to sunlight and wet and dry conditions, rainfall intensity, soil moisture and weathering, all of which control the material properties of the slope deposits (Cevik and Topal, 2003).

Slope angle is considered as the important factors and the main reason of slope instability (Haeri and Samiei, 1996; Raghuvanshi et al., 2015). In the present study it was observed that most of the past landslides have occurred in the slope class 30 - 45^{o}. The possible reason for the dominance of past landslides in this slope class is related to the poor characteristics of lithology within this slope class. The lithologys which predominantly occupy this slope class are weathered basalt, colluvial and pyroclastic deposit. Such lithology are highly disintegrated and posses poor shear strength, high porosity and permeability (Raghuvanshi et al., 2015). Thus, gravity can interact more strongly in slope instability especially on weakly consolidated masses (Shadfar *et al.*, 2005).

Studies have showed that elevation has an important influence on the occurrence of landslide. In the present study results has showed that the past landslides in the area are more dominated in elevation class 1815 – 2150 m. Apart from influence of other causative factors one major reason for dominance of landslides in this elevation range is related to the fact that much of the slopes in this elevation range are occupied by agricultural land. The results of the present study also showed that highest number of past landslides in the area was recorded within agricultural land. The agricultural land in the study area is generally located on gentle slopes and is mostly occupied by colluvial material. Poor irrigation and frequent plowing makes colluvial material loose and saturated which reduces the shear strength considerably (Raghuvanshi et al., 2015). Thus, such material becomes more prone for instability.

The landslide hazard zonation map prepared during the present study clearly indicates that the majority of the study area 78.38km^2 (36.3%) fall within very low hazard (VLH) zone. The VLH zones are dominated in Northern, eastern and southern parts of the study area. The LH zones which covers 72.85km^2 (34.2%) of the study area are dominated in western and southern parts with scattered distribution in central and northern and northeastern parts. Further, VHH zones which cover 12.78 km^2 (6.6%) of the study area are dominated in south western, western and central parts of the study area. HH zones with area coverage of 32.72 km^2 (15.4%) have scattered distribution in western, central, northwestern and south western portions.

According to the international landslide classification (Varnes 1984) predominant types of the slope processes in the study area are rotational slides, earth-flows, debris flow and rock-falls. Displacements occur when the bodies of these shallow landslides suffer abrupt changes in the pore pressure regime, which is chiefly triggered by a heavy rainfall in combination with the high slope cut during road construction (Kirche *et al*., 2000). In the present study area most of the area near to the Arbaminch Gidole Konso road fall into very high and high hazard classes. The massive landslide in the area is a result of unplanned slope cuttings for the road construction. Steep slope cut during the road construction and water saturation leads to increase in slope instability.

The analyzed deformation time-series reveal the presence of displacement from 15 up to -19 mm/year in the velocity of landslide movement for the slopes. The PS-InSAR results showed that the process of surface displacement in the area is still active. In addition, the change in the direction of movement to up lift in the mid of 13/02/2015 and 09/03/2015 at all points in the time series. The probable factor responsible for the upward movement is associated with high rainfall. Rainfall can rapidly and dramatically increase the soil moisture, causing apparent ground uplift signals on interfrograms (Hinzman *et al*., 1991).

In this study, PS-InSAR was applied to sentinel 1A SLC data to assess the surface instability on the Gidole landslide. The result indicates the current instability of the study area. The area is sparsely populated, thus the landslides do not pose major threat to human life and animals however, Kubaya and Wolayite villages are partly surrounded by potentially dangerous landslides, which can affect the infrastructure, agricultural land and may cause primarily material damage. The current instability of Gidole landslide might result from a combined of geology, high slope excavation during road construction, precipitation rate and high elevation

difference. Thus, the PS-InSAR and GIS-based methodology for integration of various topographic, geological, structural, land-use/land-cover and other datasets is quite suitable for developing a landslide hazard zonation map and slope instability assessment.

*****

CHAPTER SEVEN CONCLUSION AND RECOMMENDATIONS

7.1 Conclusion

Landslide Hazard zonation provides fundamental information for hazard assessment and monitoring strategies. In mountainous area like Gidole, direct ground based landslide triggering factor mapping and evaluation is expensive and virtually impossible within a short period of time. Remote sensing and GIS techniques provide powerful alternatives for detecting, identifying and monitoring landslides and their related factors.

Based on the results and discussion the following conclusions are forwarded:

- In order to delineate landslide hazard zones in the present study area six triggering factors were considered namely; aspect, slope, elevation, NDVI, lithology and land use/ land cover. The thematic maps of triggering factors including slope angle, lithology, aspect, elevation, LULC and NDVI were prepared from the SRTM DEM at 30m resolution and Landsat 8 OLI image, respectively. Lithology layer of the study area was extracted from the geological map of Ethiopia with the scale of 1:25,000 and through field observations made during the present study. Later, all vector maps were transformed into raster data for further analysis.

- In order to establish relational statistical correlation of various causative factors with past landslides in the area landslide inventory was made through field observations and Google earth image interpretation. In total 39 past landslides were identified in the study area. Further, Information Value (IV), a bivariate statistical analysis method was applied in which information values of predisposing causative factors were used to characterize the possibility of landslide occurrence.

- The information values are determined for each subclass of landslide related parameter on the basis of presence of landslide in the given mapping unit. The causative factor maps were combined with landslide map in order to get weight of each class. Thus, spatial relationship between the occurrence of landslides and each landslide causative factor class was derived.

- The relationship between past landslides in the study area and the triggering factors that were considered revealed that these factors affect the slope instability with

different spatial tendencies. It can be conclude that the distribution of landslide is largely governed by a combination of geo-environmental conditions. Based on information values it is concluded that Southwest facing slopes have higher probability for instability. Similarly, slopes with inclination 30 – 45^{o} are more prone for instability. Slopes falling within elevation class 1815-2150m have higher probability for failure. Majority of past landslides were observed in agricultural land and slopes which have colluvial deposits are more susceptible for failures.

- The relation analysis is the information value of the area where landslides occurred to the total area, if the value is higher relative to other classes, it shows a higher correlation; if lower, it indicates a lower correlation. Classification determines the spatial distribution of landslide on equal area classes. Therefore, the pixels of landslide susceptibility values were divided in to five classes very high hazard (VHH), high hazard (HH), moderate hazard (MHH), low hazard (LH) and very low hazard (VLH) zone by quintile (equal area) classification.

- The landslide hazard zonation map thus prepared clearly indicates that the majority of the study area 78.38km^2 (36.3%) fall within very low hazard (VLH) zone and 72.85km^2 (34.2%) of the area fall within low hazard (LH) zone. Perusal of results further shows that 12.78 km^2 (6.6%), 32.72 km^2 (15.4%) and 15.89 km^2 (7.5%) of the area falls into very high hazard (VHH), high hazard (HH) and moderate hazard (MH), respectively. Further, validation of LHZ map with past landslide inventory data shows that 92.3% of the existing landslides fall in very high hazard (VHH) and high hazard (VHH) zone. Thus, it can safely be concluded that the hazard zones delineated in the present study validates with the past landslide data and the potential zone depicted can reasonably be applied for safe planning of the area.

- Regarding slope instability assessment, it has been demonstrate that PS-InSAR is applicable form mm scale surface deformation monitoring in the study area. By analyzing dataset of Sentinel 1A SLC radar image covering the Gidole landslide, the ground displacement from −19.2 mm/yr. up to 15.3 mm/yr. away and toward LOS direction has been detected between years 2014−2018.

7.2 Recommendations

Based on the present research study findings the following recommendations are forwarded;

- The constructed of Arbaminch-Gidole-Konso asphalt road in the area has caused the reactivation of old landslide and formation of new landslides. The present study revealed that much of this road section and the surrounding areas fall within very high hazard and high hazard zones. The foundation material of the abandoned road has composed of colluvial deposit and weathered and fractured basalt. The area doesn't seem stable to load heavy structures including asphalt road. Therefore the local administrator and Ethiopian Roads Authority should consider other easily maintainable road construction option such as gravel road.

- Along the road some slopes cut require immediate rehabilitation by constructing retaining wall, using surface drainage, vegetation and slope dressing.

- The area delineated as very high hazard, high hazard and moderate hazard has a probability for future landslide and related slope instability problems. Therefore, it is recommended that prior to any future infrastructure development and settlements in these zones more detailed slope studies needs to be carried out.

- This landslide hazard zonation map can be used for optimum land management by decision makers, land use planners and engineers to decrease losses caused by current and also future landslides.

*****

REFERENCES

Ahmed S. (2009). Slope Stability Analysis Using GIS and Numerical Modeling Techniques. Unpublished MSc Thesis, Vrije Universiteit, Brussel, 120pp.

Albertz, J. and Wiggenhagen, M. (2009). Guide for Photogrammetry and Remote Sensing. 5th ed.; Wichmann: Paderborn, Germany. 334 pp

Anbalagan, R., (1992). Landslide hazard evaluation and zonation mapping in mountainous terrain. *Eng. Geol.***32**: 269-277

Aleotti, P. and Chowdhury, R., (1999). Landslide Hazard Assessment: Summary, Review and New Perspectives, *Bull Eng. Geol. Environ*. **58**: 21–44.

Bamler, R., and Hartl, P.(1998). Synthetic aperture radar interferometry. *Inverse Problems*. **14** (4): 1– 54.

Barlow, J., Franklin, S. and Martin, Y. (2006). High spatial resolution satellite imagery, DEM drivatives and image segmentation for the detection of wasting processes. *Photogrammetric engineering and remote sensing*.**72**(6): 687−692.

Barredo, J.I., Benavides, A., Hervas, J., and Van Westen C.J. (2000). Comparing Heuristic Landslide Hazard Assessment Techniques using GIS in the Tirajana Basin. Gran Canaria.

Bekele Abebe, Dramis, F., Fubelli G., Mohammed Umer, and Asfawossen Asrat, (2010). Landslides in the Ethiopian highlands and the Rift margins.*J. Afr. Ear. Sc.* **56**:131–138.

Berardino, P., Fornaro, G., Lanari, R., and Sansosti, E. (2002). A new algorithm for surface deformation monitoring based on small baseline differential SAR interferograms. *IEEE Trans. on Geosci. Remote Sensing*, **40**(11), 2375‑2383.

Berardino, P., Costantini, M., Franceschetti, G., Iodice, A., Pietranera, L. and Rizzo, V. (2003). Use of differential SAR interferometry in monitoring and modeling large slope instability at Maratea (Basilicata, Italy).*Engineering Geology*. **68**: 31–51.

Borghuis, A.M., Chang, K. and Lee, H.Y. (2007). Comparision between authomated and manual mapping of typhoon-triggered landslide from SPOT-5 imagery. *International journal of remote sensing*.**28**(7-8): 1843−1856.

Birhanu Ermias, Raghuvanshi, T.K, Abebe, B. (2017). Landslide Hazard Zonation (LHZ) around Alemketema Town, North Showa Zone, Central Ethiopia - A GIS based expert evaluation approach, *Int. Jr. Earth Sci. & Engg*. **10** (1): 33 -44.

Borghuis, A.M., Chang, K. and Lee, H.Y. (2007). Comparision between authomated and manual mapping of typhoon-triggered landslide from SPOT-5 imagery. *International journal of remote sensing*. **28**(7-8): 1843−1856.

Brenning A. (2005). Spatial prediction models for landslide hazard: review, comparison and evaluation. *Natural hazard and Earth system science*. **5**: 853-862

Carrara, A., Cardinali, M., and Guzzetti, F. (1992). Uncertainty in assessing landslide hazard and risk.*ITC J.* **2**: 172–183.

Çevik, E., and Topal, T. (2003) GIS-based landslide susceptibility mapping for a problematic segment of the natural gas pipeline, Hendek (Turkey).*Environ. Geol*. **44**: 949–962.

Chau, T., Sze, Y. Fung, M. Wong, W., Fong, E. and Chan, L.(2004). Landslide Hazard Analysis for Hong Kong Using Landslide Inventory and GIS.*Computers & Geosciences***30**(4): 429–443.

Chauhan, S., Mukta, S Arora, M. and Gupta, N. (2010). Landslide Susceptibility Zonation through Ratings Derived from Artificial Neural Network. *International Journal of Applied Earth Observation and Geoinformation.***12** (5): 340–350.

Colesanti, C., and Wasowski, J. (2006). Investigating landslides with space-borne Synthetic Aperture Radar (SAR) interferometry.*Engineering Geology*. **88**: 173–199.

Cruden, D.M. (1991). A simple definition of a landslide.*Bulletin of the International Association for Engineering Geology.* **43**:27−29.

Cumming, I. and Wong, F. (2005). Digital processing of SAR data. 685 Canton Street, Norwood, MA 02062: Artech House, Inc.

Davidson, A .(1983). The Omo River Project, Ministry of Mines and Energy, (EIGS), p. 89 (1:250000 and 1:500000 geological maps)

Fall, M., Azzam, R. and Noubactep, C. (2006). A multi-method approach to study the stability of natural slopes and landslide susceptibility mapping. Eng.Geol.82:241-263.

Ferretti, A., Prati, C. and Rocca, F. (2000). Nonlinear subsidence rate estimation using permanent scatterers in differential SAR interferometry.*IEEE Trans. on Geosci and Remote Sensing*. **38** (5): 2202–2212.

Ferretti, A., Prati, C. and Rocca, F. (2001). Permanent scatterers in SAR interferometry.*IEEE Trans. on Geosci. Remote Sensing*. **39**(1): 8–20.

Fikre Girma, Raghuvanshi, T.K., Tenalem Ayanew, and Trufat Hailemariam (2015). Landslide hazard zonation in Ada Berga district, Central Ethiopia – A GIS based statistical Approach.*Journal of Geomatics*. **9**:1−14.

Gemechis Chimidi, Raguvanshi. T.K., Suryabhagavan, K.V. (2017). Landslide hazard zonation in and around Gimbi town, Western Ethiopia-a GIS statistical approach. Appl Geomat. **9 (4)** :219–236.

Goldstein, R. M. and Zebker, H.A. (1987) Interferometric radar measurement of ocean surface currents.*Nature*. **328** (6132):707–719.

Goldstein, R.M. and Zebker, H.A. (1989). Mapping small elevation changes over large areas: Differential Radar interferometry, *J.Geophys. Res*. **94:** 9183–9191.

Greif, V. and Vlcko, J. (2012). Monitoring of post-failure landslide deformation by the PS-InSAR technique at Lubietova in Central Slovakia.*Environ. Earth Sci.* **66**: 1585–1595.

Guzzeti, F., Carrara, A., Cardinali, M. Reichenbach, P. and Carrara, A. (2000). Comparing landslide maps: A case study in the upper Tiber river basin, central Italy. *Environmental management*. **25**(3): 247−263.

Guzzetti, F., Reichenbach, P., Cardinali, M., Galli, M. and Ardizzone, F. (2005). Landslide hazard assessment in the Staffora basin, Northern Italian Apennines. *Geomorphology.* **72**: 272–299.

Haeri, S.M. and Samiei, A.H.(1996). New zoning approach of slope areas against the landslide risk with emphasis on zoning of Mazandaran province.*Earth Sciences*, No. 23.

Hanssen, R. F. (2001). Radar Interferometry Data Interpretation and Error Analysis. *Springer*. 328 pp.

Hanssen, R.F. (2004). Stochastic Modeling of Times Series Radar Interferometry. **In**: International Geoscience and Remote Sensing Symposium. IGARSS'04, Anchorage, Alaska, 20–24 September.

Henok Woldegiorgis, Raghuvanshi T.K. and Balamwal Atnafu (2014). Landslide hazard zonation using expert evaluation technique: a case study of the area between Gohatsion town and the Abay (Blue Nile) River, Central Ethiopia.*SINET: Ethiopian Journal of Science.* **37**(2): 75−94.

Highland, L.M. and Bobrowsky, P. (2008). The Landslide Handbook- A Guide to Understanding Landslides. U.S. Geological Survey, Reston, Virginia, 147 pp.

Hilley, G. E., Burgmann, R., Ferretti, A., Novali, F. and Rocca, F. (2004). Dynamics of slow moving landslides from permanent scatterer analysis.*Science*, **304**(5679), 1952–1955.

Hinzman, L., Kane, R., Gieck, E. and Everett, K. (1991). Hydrologic and thermal properties of the active layer in the Alaskan Arctic, Cold Reg. *Sci. Technol*. **19**(2), 95–110.

Hooper, A., Segall, P. and Zebker, H. (2007). Persistent scatterer InSAR for crustal deformation analysis, with application to Volcán Alcedo, Galapagos, *J. Gephys. Res*. **112**: 740−752.

https://joshuaproject.net/people_groups/11887/ET accessed on 14/03/2018

Hungr, O., Evans, S. G., Bovis, M. J. and Hutchinson, J. N. (2001). A review of the classification of landslides of the flow type.*Environmental and Engineering Geoscience*. **7**(3), 221–228.

Jiri Sima (1987). Hydrogeology and Hydrochemistry of the Bako and Ist'ifanos Hayk areas NB 37 – 9 and NB 37 – 13, EIGS, Note No. 271.

Kanungo, D. P., Arora, M. K., Sarkar, S. and Gupta, R. P. (2009). Landslide Susceptibility Zonation Mapping – a review.*Journal of south Asia disaster studies*. **2**:1−81.

Kifle Woldaregay (2013). Review of the occurrences and influencing factors of landslides in the highlands of Ethiopia.*Momona Ethiopian Journal of Science*. **5**(1):3−31.

Kircher K., Krejčí O., Máčka Z. and Bíl M. (2000). Slope deformations in eastern Moravia, Vsetín District(Outer Western Carpathians). Acta Universitas Carolinae, vol. 35, pp. 133−143.

Lanari, R., Casu, F., Manzo, M., Zeni, G., Berardino, P., Manunta, M., Pepe, (2007) A. An overview of the small baseline subset algorithm: A DInSAR technique for surface deformation analysis.*Pure Appl. Geophys.***164**: 637–661.

Lillesand, T, R. W. Kiefer, and J Chipman. (2007). Remote Sensing and Image Interpretation. 6th ed. John Wiley & Sons Inc.

Lulseged Ayalew, (1999). The effect of seasonal rainfall on landslides in the highlands of Ethiopia. *Bull. Eng. Geol. Environ*. **58**: 9–19.

Lulseged Ayalew and Yamagishi, H. (2004). Slope failure in the Blue Nile basin, as seen from landscape evolution perspective. *Geomorphology* **57**: 95–116.

Lulseged Ayalew, Yamagishi H, Marui H, and Kanno, T. (2005). Landslide in Sado Island of Japan: Part II. GIS-based susceptibility mapping with comparison of results from two methods and verifications.*Eng Geol.***81**:432–445.

Malet, J.P., Maquaire, O. and Calais, E. (2002). The use of global positioning system techniques for the continuous monitoring of landslides – application to the super – sauze earth flow (Alpes de Haute- Provence, France). *Geomorphology***43**:33–54

Martha, T.R., Kerle,N., Jetten, V., Van Westen, C.J. and Vinod Kumar, K. (2010). Characterizing spectral, spatial and morphometric properties of landslides for automatic detection using object-oriented methods.*Geomorphology*.**116**: 24−36.

Moccia, A. and Rufino, G. (2001). Spaceborne along-track SAR interferometry: Performance analysis and mission scenarios, *IEEE Trans. Aerosp. Electron. Syst*. **37**: 199–213.

Nichol,J. and Wong, M.S (2005). Satellite remote sensing for detailed landslide inventories using change detection and image fusion.*International Jornal of remote sensing*. **26**(9): 1913−1926.

Raghuvanshi, T.K., JemalIbrahim, and DerejeAyalew, (2014). Slope stability susceptibility evaluation parameter (SSEP) rating scheme – An approach for landslide hazard zonation.*J. Afr. Earth Sci*. **99**: 595−612.

Raghuvanshi, T.K., LensaNegassa, and Kala, P.M. (2015). GIS based Grid Overlay Method versus Modeling Approach – A Comparative Study for Landslide Hazard Zonation (LHZ) in Meta Robi District of West Showa Zone in Ethiopia. Egypt. J. *Remote sensing Space Sci.* **18**: 235−250.

Richman, D., (1971).Three dimensional azimuth-correcting mapping radar, Tech. rep., USA: United Technologies Corporation.

Rott, H. and Nagler, T. (2006). The contribution of radar interferometry to the assessment of landslide hazards.*Advances in Space Research*. **37**: 710–719.

Rott, H., Scheuchl, B., Siegel, A. and Grasemann, B. (1999). Monitoring very slow slope movements by means of SAR interferometry: A case study from a mass waste above a reservoir in the Ötztal Alps, Austria.*Geophys. Res. Lett.* **26:** 1629–1632.

Rouse, J.W., Haas, R.H., Schell, J.A. and Deering, D.W. (1974) Monitoring vegetation systems in the Great Plains withERTS. **In**: Third Earth Resources Technology Satellite–1 Syposium, Volume I: Technical Presentations, NASA SP-351; Freden, S.C., Mercanti, E.P., Becker, M., Eds.; NASA: Washington, DC, USA, pp. 309–317.

Sansosti, E., Berardino, P., Manunta, M., Serafino, F. and Fornaro, G. (2006). Geometrical SAR image registration.*IEEE Trans. on Geosci. Remote Sensing*. **44**(10): 2861–2870.

Shadfar, S., Norouzi, A.A., Ghodosi, J. and Ghayumian, J. (2005). Zoning landslide hazard in the basin of Laktrash, *Sci. J. Soil Water Cons*. **1**: 1–10.

Shiferaw Ayele, Raghuvanshi, T.K. and Kala, P.M. (2014). "Application of Remote Sensing and GIS for Landslide Disaster Management - A case from Abay Gorge, Gohatsion – Dejen Section, Ethiopia" In: Landscape Ecology and Water Management, Proceedings of International Geographical Union (IGU) Rohtak Conference, Vol-2, Advances in Geographical and Environmental Sciences, (Singh, M, Singh, R.B, Hassan, M.I. eds.), Springer Japan, pp 15−32. (doi:10.1007/978-4-431-54871-3_2), http://link.springer. com/book/10.1007/978-4-431-54871-3

Skolnik, M. L. (2001). Introduction to RADAR systems. 3 edn. 1221 Avenue of the Americas, New York, NY 10020: Tata McGraw-Hill.

Strozzi, T., Farina, P., Corsini, A., Ambrosi, C., Th¨uring, M., Zilger, J., Wiesmann, A., Wegm¨uller, U. and Werner, C. (2005). Survey and monitoring of landslide displacements by means of L-band satellite SAR interferometry.*Landslides*. **2**(3):193–201.

Suchandt, S., Runge, H., Breit, H., Steinbrecher, U., Kotenkov, A. and Balss, U. (2010). Automatic Extraction of Traffic Flows Using TerraSAR-X Along-Track Interferometry.*IEEE Trans. Geosci. Remote Sens.***48:** 807–819.

Tenalem Ayenew and Barbieri, G. (2005). Inventory of Landslides and Susceptibility Mapping in the Dessie area, Northern Ethiopia.*Engineering Geology*. **77**: 1−15.

Terlien, M.(1996). Modeling spatial and temporal variations in rainfall-triggered landslides. Ph.D. thesis, ITC Publ. Nr. 32, Enschede, The Netherlands, 254 pp.

Tilahun Hamza and Raghuvanshi. T.K., (2017) GIS based Landslide Hazard Evaluation and Zonation - A case from Jeldu District,Central Ethiopia.*Journal of King Saud University – Science*. **29(2):**151−165.

Torres, R., Snoeij, P., Geudtner, D., Bibby, D., Davidson, M., Attema, E., Potin, P., Rommen, B. and Floury, N. (2012). GMSE Sentinel – 1 mission. *Remote Sens. Enviro*. **120**:9-24

Tsion Aragaw. (2017). An integrated expert evaluation and statistical approach for Landslide hazard evaluation and zonation – A case along Alemketema – Fetra Route corridor, Northern Showa Zone, Central Ethiopia,GIS based expert evaluation, Unpublished MSc Thesis, Addis Ababa University, Addis Ababa, Ethiopia. P 108.

Van Westen, C.J., Van Asch, T. W. J. and Soeters, R. (2006). Landslide hazard and risk zonation - why is it still so difficult? *Bull. Eng. Geol. Env*. **65**: 167–184.

Van Westen, C.J., Castellanos, E., Sekha and Kuriakose, L. (2008). Spatial Data for Landslide Susceptibility, Hazard, and Vulnerability Assessment: An Overview.*Engineering Geology.* **102** (3-4): 112–131.

Varmuza K. and Filzmoser P. (2009) Introduction to multivariate statistical analysis in chemometrics.Taylor & Francis, Boca Raton, USA, 321pp.

Varnes, D.J. (1978). Slope movements types and processes. **In**: Schuster, R.L., Krizek, R.S. (Eds.), Landslides: Analysis and Control. Transportation Research Board, National Academy of Sciences, Special Report 176, 2, Washington, DC, pp. 20–47.

Varnes, D. J. (1984). Landslide hazard zonation: a review of principles and practice, The International Association of Engineering Geology Commission on Landslide and Other Mass Movements on Slopes, United Nations Educational, Scientific and Cultural Organization (UNESCO), 7 place de Fontenoy, 75700 Paris, France, 60 pp.

Wachal, D.J. and Hudak, P.F. (2000). Mapping landslide susceptibility in Travis County, Texas, USA. *GeoJournal*. **51**:245−253.

Wadge, G.(1988). The potential of GIS modelling of gravity flows and slope instabilities. *Int. J. Geographic Information Systems.***2**(2): 143–152.

Xu, Chong, Fuchu Dai, Xiwei Xu and Yuan Hsi Lee. (2012). GIS-Based Support Vector Machine Modeling of Earthquake-Triggered Landslide Susceptibility in the Jianjiang River Watershed, China.*Geomorphology.* **145-146**: 70–80.

Yin, K.L. and Yan, T.Z. (1988). Statistical Prediction Models for Slope Instability of Metamorphosed Rocks. ***In:*** *Proceedings of the 5th International Symposium on Landslides*, pp. 1269– 1272. Lausanne, Switzerland.

Zan, F. and Guarnieri, A.M. (2006). TOPSAR: Terrain observation by progressive scans.*IEEE Trans. Geosci. Remote Sens.***44**: 2352–2360.

Zebker, H. A. and Goldstein, R. M. (1986). Topographic mapping from interferometric synthetic aperture radar observations.*J. Geophys. Res.***91**(B5): 4993–5000.

Zebker, H. A. and Villasenor, J. (1992). Decorrelation in interferometric radar echoes.*IEEE Trans. on Geosci. Remote Sensing*. **30**(5):950–959.

Zebker, H. A., Rosen, P. A. and Hensley, S. (1997). Atmospheric artifacts in interferometric synthetic aperture radar surface deformation and topographic maps.*J. Geophys. Res.***102**, 7547–7563.

Zerihun Dawit. (2016). Landslide Hazard Evaluation and Zonation in the area Kindo Didaye, South West Ethiopia, Unpublished MSc Thesis, Addis Ababa University, Addis Ababa, Ethiopia. P 118.

Zisk, S. H. (1972) A new Earth-based radar technique for the measurement of lunar topography.*Moon*. **4** (3/4): 296–306.

*****

APPENDIX

APPENDIX 1: GPS points for landslide inventory

S/N	Easting	Northing
1	5°40' 2"	37 °22'12"
2	5°40'00"	37°21'49"
3	5°39'41"	37°21'37"
4	5° 39'36"	37°21'41"
5	5°39'38"	37°21'49"
6	5°39'47"	37°21'54"
7	5°39'40"	37°21'57"
8	5°40'00"	37°22'5"
9	5°40'23"	37°22'12"
10	5°40v11"	37°22'14"
11	5°40'5"	37°22'10"
12	5°40'10"	37°22'22"
13	5°40'23"	37°21'34"
14	5°39'54"	37°21'13"
15	5°39'1"	37°22'35"
16	5°39'10"	37°22'42"
17	5°39'4"	37°22'44"
18	5°38'38"	37°22'59"
19	5°38'25"	37°23'7"
20	5°38'14"	37°23'0"
21	5°38'13"	37°23'19"
22	5°37'53"	37°23'38"
23	5°37'45"	37°23'43"
24	5°37'43"	37°24'0"
25	5°37'35"	37°23'56"
26	5°37'25"	37°23'52"
27	5°37'23"	37°23'49"
28	5°37'23"	37°23'57"
29	5°37'7"	37°23'55"
30	5°37'2"	37°23'54"
31	5°37'20"	37°22'9"
32	5°39'50"	37°21'56"
33	5°39'39"	37°21'58"
34	5°40'11"	37°22'24"
35	5°39'2"	37°22'34"
36	5°39'7"	37°22'45"
37	5°38'21"	37°23'7"
38	5°38'13"	37°23'23"
39	5°37'44"	37°23'43"

APPENDIX 2: Landslide inventory field photo and Google earth image

Landslide Field Photographs

Landslides – Google Earth Images

APPENDIX 3: Rainfall data of Gidole Station

Station Name	Year	Jan	Feb	Mar	Apr	May	Jun	Jul	Aug	Sep	Oct	Nov	Dec	Annual Rainfall
Gidole	2008	31.1	45.3	120.4	178.1	201.3	89.1	97.6	112.4	121	171.3	101.2	93.4	1362.2
Gidole	2009	46.3	51.4	115.4	169.2	194.1	80.9	91.6	108.4	112.8	160	91.8	86.4	1308.3
Gidole	2010	58.6	57.2	125.6	173.5	208.6	97.6	101.8	128.9	131.8	164.7	82.6	91	1421.9
Gidole	2011	4.5	9.5	43.2	68.4	270.4	115.4	202.8	201.9	106.6	25.2	138.4	10.5	1196.8
Gidole	2012	1.2	48.9	24.1	201.2	139.3	89	314.3	246.4	138.8	29.1	89.7	27.2	1349.2
Gidole	2013	41	10.5	31.6	348.9	81.6	167.2	261.8	232.9	129.4	79.5	45.6	0	1430
Gidole	2014	51	50	129.4	91.1	236.1	134.9	190.7	120	178.9	160	121.2	14.9	1478.2
Gidole	2015	99.5	73	213.6	209.7	332.2	118.4	242.9	144.5	153.5	107.2	128.3	39.1	1861.9
Gidole	2016	49.8	25.1	120.3	167.9	235.8	304.1	205.3	236.4	185.2	27.6	32.1	29.8	1619.4
Gidole	2017	36.1	54.6	60	73	81	85.7	92.6	120	115.8	176.9	91.6	33.8	1021.1
	Avg	41.91	42.55	98.36	168.1	198.04	128.23	180.14	165.18	137.38	110.15	92.25	42.61	1404.9

APPENDIX 4: Selected Points for displacement Time series plot

S/N	Point	Latitude	longtiude
1	A	5.66	37.35
2	B	5.66	37.36
3	C	5.66	37.37
4	D	5.64	37.38

APPENDIX 5: Accuracy assessment for land-use and land-cover classification

	Agricultural land	Built-up area	Forest	Bare-land	Bush/Shrub land	Total	User accuracy
Agricultural land	61	3	0	2	4	70	87.14
Built-up	3	45	2	0	0	50	90.00
Forest	1	0	39	0	2	42	92.86
Bare-land	3	0	0	28	1	32	87.50
Bush/shrub land	1	0	3	0	22	26	84.62
Total	69	48	44	30	29	220	
Producer Accuracy	88.40	93.75	88.63	93.33	75.86	Correctly classified =195	
	Overall accuracy= 88.64%			**Kappa Coefficient=0.85**			

*****